

# Galaxy evolution in nearby galaxy groups. III. A *GALEX* view of NGC 5846, the largest group in the local universe

Antonietta Marino<sup>1</sup>\*, Paola Mazzei<sup>1</sup>, Roberto Rampazzo<sup>1</sup>, Luciana Bianchi<sup>2</sup>

<sup>1</sup>INAF Osservatorio Astronomico di Padova, vicolo dell’Osservatorio 5, I-35122 Padova, Italy

<sup>2</sup>Dept. of Physics and Astronomy, Johns Hopkins University, 3400 North Charles Street, Baltimore, MD 21218 USA

Accepted. Received

## ABSTRACT

We explore the co-evolution of galaxies in nearby groups ( $V_{hel} \leq 3000 \text{ km s}^{-1}$ ) with a multi-wavelength approach. We analyze *GALEX* far-UV (FUV) and near-UV (NUV) imaging, and SDSS u,g,r,i,z data of groups spanning a large range of dynamical phases. We characterize the photometric properties of spectroscopically-confirmed galaxy members and investigate the global properties of the groups through a dynamical analysis.

Here we focus on NGC 5846, the third most massive association of Early-Type Galaxies (ETG) after the Virgo and Fornax clusters. The group, composed of 90 members, is dominated by ETGs (about 80 per cent), and among ETGs about 40 per cent are dwarfs. Results are compared with those obtained for three groups in the LeoII cloud, which are radically different both in member-galaxy population and dynamical properties. The FUV-NUV cumulative colour distribution and the normalized UV luminosity function (LF) significantly differ due to the different fraction of late-type galaxy population.

The UV LF of NGC 5846 resembles that of the Virgo cluster, however our analysis suggests that star-formation episodes are still occurring in most of the group galaxies, including ETGs. The NUV-i colour distribution, the optical-UV colour-colour diagram, and NUV-r vs.  $M_r$  colour-magnitude relation suggest that the gas contribution cannot be neglected in the evolution of ETG-type group members. Our analysis highlights that NGC 5846 is still in an active phase of its evolution, notwithstanding the dominance of dwarf and bright ETGs and its virialized configuration.

**Key words:** galaxies: group: individual: NGC 5846 group, USGC U677 – Ultraviolet: galaxies – galaxies: formation – galaxies: evolution – galaxies: photometry – galaxies: kinematics and dynamics.

## 1 INTRODUCTION

The study of the co-evolution of galaxies in groups is crucial to address the problem of the star formation quenching and galaxy morphological transformations, as groups contain most ( $\sim 60$  per cent) of the galaxies in the universe at the present day (e.g. Tully 1988; Ramella et al. 2002; Eke et al. 2004; Tago et al. 2008), and most of the stellar mass is formed in groups. The transition between galaxy properties typical of field and clusters happens just at the characteristic densities of groups, suggesting the existence of evolutionary mechanisms acting before galaxies in groups fall into clusters (Lewis et al. 2002; Gómez et al. 2003). Such

re-processing mechanisms act by transforming field, i.e. spiral galaxies, to cluster-like galaxies, i.e. ETGs, and basically drive groups from an “active” (star forming) phase, typical of field, to a more “passive” phase, typical of clusters (e.g. Goto et al. 2003; Gómez et al. 2003). Evidence in this sense comes from a number of “classical” studies on the impact of environment on galaxy properties showing that ETGs are more strongly clustered than late-type galaxies (e.g. Davis & Geller 1976). Dressler (1980) showed that the fraction of elliptical and S0 galaxies is higher in denser environments. By now, it is widely accepted that galaxies in clusters tend to have depressed star formation rates (SFRs) in comparison with the field population (e.g. Balogh et al. 2004; Poggianti et al. 2006, and references therein). Several physical processes are believed to play a role in

\* E-mail: antonietta.marino@oapd.inaf.it

galaxy evolution and star formation variations. They have been inferred both from observations and simulations and there is a wide consensus that they are different in rich and poor galaxy environments. Mergers can transform spirals into ellipticals (Toomre & Toomre 1972; Barnes 2002), and quench star formation by ejecting the interstellar medium via starburst, AGN or shock-driven winds (e.g. Di Matteo et al. 2005). Since velocity dispersions of groups are comparable to the velocity dispersion of individual galaxies, both interactions and merging are more favored in groups than in clusters (Mamon 1992) as well as phenomena like “galaxy strangulation” (Kawata & Mulchaey 2008). Transforming mechanisms in rich environments should act through galaxy-galaxy “harassment” and ram-pressure (see e.g. Moore et al. 1996).

The dramatic evidence of galaxy transformation has been obtained with GALEX. UV - optical colour magnitude diagrams (CMD) evidenced not only a sequence of red galaxies, mostly ETGs, and a “blue cloud” mainly composed of late-type galaxies, but also a intermediate region, the “green valley”, populated of transforming galaxies (Schawinski et al. 2007).

We are exploring the co-evolution of galaxies in groups in the local Universe by adopting a multi-wavelength approach. We use UV and optical imaging to analyze a set of nearby groups spanning a large range of evolutionary phases. In particular, GALEX UV wide-field imaging, made it possible to directly map present-day star formation, ranking groups according to their blue and red galaxy population. Moreover, we analyze group compactness, a signature of the evolutionary phase, through a kinematic and dynamical analysis. To further investigate the transition from active groups to more evolved passive systems, we select groups with different properties, from late-type galaxy dominated groups, analogs of our Local Group (Marino et al. 2010, hereafter Paper I), to groups with an increasing fraction of ETGs, increasing signatures of interaction, and advanced stage of virialization (Marino et al. 2013, hereafter Paper II).

In order to investigate the transition between active groups and more evolved passive systems we analyze in this paper the NGC 5846 group, that in the Ramella et al. (2002) catalogue is labeled as USGC U677.

Ferguson & Sandage (1991) showed that the dwarf-to-giant ratio increases with the richness of the group. Eigenthaler & Zeilinger (2010) estimated the early-type-dwarf-to-giant-ratio (EDGR) (i.e. dE+dE,N+dS0 to E+S0) for NGC 5486 group obtaining EDGR=2.69. In the Local Supercluster, this value is exceeded only by Virgo (EDGR=5.77) and Fornax (EDGR=3.83) clusters indicating that NGC 5846 is the third more massive galaxy aggregate. The group is dominated by two bright ETGs, NGC 5846 and NGC 5813, that do not show clear signatures of interaction in UV and optical images. X-ray studies revealed the presence of an extended (50 – 100 kpc radius) halo of NGC 5846, and numerous peculiar features, cavities and bubbles in both galaxies (Trinchieri & Goudfrooij 2002; Mulchaey et al. 2003; Werner et al. 2009; Machacek et al. 2011; Randall et al. 2011; Werner et al. 2014). These two X-ray halos suggested the presence of sub-structures in the NGC 5846 group and motivated a wide literature about the determination of

group members (e.g. Tully 1987; Haynes & Giovanelli 1991; Nolthenius 1993; Giuricin et al. 2000; Ramella et al. 2002; Mahdavi et al. 2005; Eigenthaler & Zeilinger 2010). The low optical luminosity galaxy population has been studied by Mahdavi et al. (2005) and Eigenthaler & Zeilinger (2010): nucleated dwarfs reside near the bright members, and only four dwarfs show fine structures or interaction signatures. At odd, signatures of activity are found in the inner part of the two bright members. Werner et al. (2014) detected  $\text{H}\alpha + \text{[NII]}$  at kpc scale and  $\text{[CII]} \lambda = 157 \mu\text{m}$  emission in both galaxies. Rampazzo et al. (2013), using Spitzer, detected mid infrared lines like  $\text{[NeII]} \lambda = 12.81 \mu\text{m}$ ,  $\text{[NeIII]} \lambda = 15.55 \mu\text{m}$  and some  $\text{H}_2\text{O-0}$  lines in both galaxies.

Although NGC 5846 is the third most massive association of ETGs after Virgo and Fornax, its UV properties are still unknown and this motivates the present study. The paper is arranged as follows. Section 2 discusses the criteria adopted to select the galaxy members, and the group kinematical and dynamical properties. Section 3 presents the UV and optical observations and data reduction. The photometric results are given in Section 4. Section 5 and 6 focus on the discussion and our conclusions, respectively.  $H_0 = 75 \text{ km s}^{-1} \text{Mpc}^{-1}$  is used throughout the paper but for luminosity function, where in agreement with Boselli & Gavazzi (2014) a value of  $70 \text{ km s}^{-1} \text{Mpc}^{-1}$  is adopted.

## 2 MEMBERSHIP, AND DYNAMICAL ANALYSIS OF THE GROUP

### 2.1 Selection of the NGC 5846 group members

We follow the approach developed in our Paper I and II. Briefly, once characterized the group through a density analysis of a region of 1.5 Mpc of diameter around the B brightest member, we revise the group membership using recent red-shift surveys. For each member galaxy, we investigate morphology and measure surface photometry in FUV, NUV, and optical  $u, g, r, i, z$  bands.

As described in more detail in Paper II, the group sample has been selected starting from the catalog of Ramella et al. (2002) which lists 1168 groups of galaxies covering 4.69 steradians to a limiting magnitude of  $m_B \approx 15.5$ . The member galaxies of the catalog were cross-matched with the GALEX and SDSS archives in order to select groups covered by both surveys. We chose only groups within 40 Mpc, i.e. with an heliocentric radial velocity  $V_{hel} < 3000 \text{ km s}^{-1}$ , and composed of at least 8 galaxies to single out intermediate and rich structures. The above criteria led to a sample of 13 nearby groups having between 8 and 47 members listed in the catalog of Ramella et al. (2002). Their fraction of ETGs, according to the **Hyper-Lyon-Meudon Extragalactic Database** (Makarov et al. 2014, HYPERLEDA hereafter), ranges from the same fraction as in the field, i.e.  $\approx 15\text{--}20$  per cent, to a value typical of dense environments,  $\approx 80\text{--}85$  per cent (e.g. Dressler 1980). UV and optical data are available for most of their galaxy members and we further obtained new NUV imaging of most of the remaining galaxies in the GALEX GI6 program 017 (PI A. Marino). We focus here on NGC 5846 group. In the catalogue of Ramella et al. (2002) the group, named USGC U677, is composed of 17 members with  $\langle V_{hel} \rangle \sim 1634 \pm 117 \text{ km s}^{-1}$  and

**Table 1.** Journal of the galaxy members<sup>a</sup>.

Id. Nr.	Galaxy	RA (J2000) [deg]	Dec. (J2000) [deg]	Morph. type [ <sup>a</sup> — <sup>b</sup> ]	Mean Hel. Vel [km/s]	$B_T$ [mag]	$D_{25}$ ["]	$\log r_{25}$	P.A. [deg]	Incl. [deg]	E(B-V) [mag]
1	PGC053384	224.00505	2.46358	S0-a — ...	2109 ± 22	15.20 ± 0.44	58.6	0.45	171.3	90	0.038
2	PGC1186917	224.14275	1.17921	S0 — ...	1918 ± 6	17.24 ± 0.29	27.4	0.27	41.1	72.8	0.034
3	PGC1179522	224.47140	0.93426	S? — E/S0	1887 ± 39	16.90 ± 0.39	48.8	0.54	58.7	90	0.034
4	PGC184851	224.58825	1.84533	E-S0 — E	1870 ± 5	15.99 ± 0.29	0.87	0.26	85.6	80	0.041
5	SDSSJ145824.22+020511.0	224.59995	2.08630	E — dE	2369 ± 60	-	-	-	-	-	0.037
6	SDSSJ145828.64+013234.6	224.61930	1.54303	E — dE,N	1494 ± 20	17.64 ± 0.5	28.1	0.07	154.9	46	0.039
7	PGC1223766	224.67030	2.39386	E — dE,N	1559 ± 24	18.36 ± 0.41	15.1	0.07	69.1	45.4	0.036
8	PGC1242097	224.69205	2.96899	E — E	1791 ± 40	16.39 ± 0.45	23.9	0.06	129.5	40.3	0.036
9	PGC053521	224.70300	2.02350	E — E	1805 ± 2	14.87 ± 0.32	56.0	0.2	2.6	77.5	0.037
10	SDSSJ145944.77+020752.1	224.93640	2.13106	E — dE,N	1458 ± 59	18.39 ± 0.5	18.1	0.01	-	16.5	0.035
11	NGC5806	225.00165	1.89128	Sb — Scd	1348 ± 3	12.35 ± 0.06	181.2	0.27	172.5	60.4	0.039
12	PGC053587	225.06915	2.30069	S0 — S0	1819 ± 3	15.50 ± 0.26	58.6	0.4	10.1	90	0.034
13	SDSSJ150019.17+005700.3	225.08010	0.95001	E — dE, N	1961 ± 60	17.56 ± 0.5	28.1	0.07	41.2	44.1	0.042
14	NGC5846:[MTT2005]046	225.11205	1.47526	... — pec	1501 ± 60	-	-	-	-	-	0.039
15	NGC5811	225.11235	1.62362	SBm — dE	1535 ± 6	14.76 ± 0.32	61.4	0.06	96.8	31.3	0.039
16	SDSSJ150033.02+021349.1	225.13755	2.23036	E — dE	1278 ± 37	17.24 ± 0.5	33.0	0.1	31.3	58.2	0.034
17	PGC1193898	225.21915	1.40493	E — dE,N	1885 ± 10	16.87 ± 0.39	36.3	0.34	9.6	90	0.038
18	SDSSJ150059.35+015236.1	225.24705	1.87670	E — dE,N	2196 ± 48	18.76 ± 0.5	16.1	0.05	96.2	38.1	0.035
19	SDSSJ150059.35+013857.0	225.24735	1.64913	E — E	2363 ± 18	18.18 ± 0.35	17.3	0.14	14.7	68.7	0.038
20	SDSSJ150100.85+010049.8	225.25350	1.01382	E — dE/I	1737 ± 5	18.03 ± 0.35	23.9	0.21	113.6	90	0.039
21	PGC053636	225.26295	0.70764	Sb — S0/a	1724 ± 3	15.88 ± 0.29	32.3	0.11	172.6	40.5	0.043
22	SDSSJ150106.96+020525.1	225.27900	2.09031	E — dE,N	1943 ± 25	18.33 ± 0.35	20.8	0.12	154.9	62.3	0.034
23	NGC5813	225.29700	1.70201	E — E	1956 ± 7	11.52 ± 0.19	250.1	0.18	142.5	90	0.037
24	PGC1196740	225.31395	1.49826	E — dE	2139 ± 5	17.75 ± 0.39	25.1	0.13	0.9	68.3	0.039
25	PGC1205406	225.31635	1.77348	E — dE/I	1343 ± 15	18.06 ± 0.45	25.6	0.33	111.5	90	0.036
26	SDSSJ150138.39+014319.8	225.40995	1.72204	E — dE,N	2290 ± 15	17.83 ± 0.35	23.9	0.03	-	28.7	0.037
27	PGC1208589	225.41085	1.87018	E — dE,N	2152 ± 2	17.90 ± 0.62	14.7	0.09	106.5	52.5	0.034
28	UGC09661	225.51465	1.84102	SBd — Sdm	1243 ± 2	14.81 ± 0.3	62.8	0.04	139	28.5	0.034
29	PGC1192611	225.61740	1.36422	E — dE	1516 ± 55	18.49 ± 0.47	15.8	0.07	-	45.6	0.036
30	SDSSJ150233.03+015608.3	225.63750	1.93582	E — dE/I	1647 ± 60	18.18 ± 0.5	21.8	0.14	17.2	69.2	0.031
31	SDSSJ150236.05+020139.6	225.65010	2.02759	E — dE	1992 ± 20	18.11 ± 0.35	30.1	0.42	108.5	90	0.031
32	PGC1230503	225.93435	2.55236	E — dE	1782 ± 17	17.56 ± 0.35	20.8	0.14	122.2	69.1	0.032
33	SDSSJ150349.93+005831.7	225.95790	0.97651	I — dI	2002 ± 48	16.99 ± 0.5	43.5	0.22	70.8	61.7	0.037
34	PGC1185375	225.95955	1.12684	S0 — E	1575 ± 7	16.48 ± 0.35	27.4	0.17	102.8	59.3	0.034
35	PGC087108	225.98430	0.42954	I — ...	1581 ± 2	17.32 ± 0.58	26.2	0.15	179.1	50.8	0.032
36	NGC5831	226.02900	1.21994	E — E	1631 ± 2	12.44 ± 0.11	134.3	0.05	128.7	38.5	0.034
37	PGC1197513	226.03515	1.52454	S0-a — S0/a	1837 ± 2	16.43 ± 0.38	35.7	0.25	11.1	63	0.035
38	PGC1230189	226.05450	2.54297	E — E	1909 ± 7	15.89 ± 0.31	42.5	0.15	179.3	73.5	0.029
39	PGC1179083	226.09935	0.91839	E — dE	1657 ± 60	18.12 ± 0.5	18.1	0.05	127	38.4	0.034
40	PGC1216386	226.10295	2.11462	E — E	1704 ± 13	17.44 ± 0.34	28.1	0.27	97.9	90	0.034
41	NGC5846:[MTT2005]139	226.14300	1.03243	E — dE,N	2184 ± 60	-	-	-	-	-	0.034
42	PGC1190315	226.17870	1.29088	E — dE	1967 ± 9	16.96 ± 0.42	23.9	0.04	-	33.7	0.032
43	SDSSJ150448.49+015851.3	226.20225	1.98084	E — dE	1960 ± 23	18.07 ± 0.5	21.3	0.09	18.3	53.9	0.034
44	PGC1211621	226.26825	1.96462	E — E	2381 ± 2	17.60 ± 0.42	16.9	0.07	160.7	45.6	0.034
45	NGC5838	226.35960	2.09949	E-S0 — S0	1252 ± 4	11.79 ± 0.12	233.4	0.47	38.8	90	0.029
46	NGC5839	226.36455	1.63474	S0 — S0	1227 ± 32	13.69 ± 0.06	86.7	0.05	103.1	30	0.035
47	PGC1190358	226.36890	1.29233	I — dE	2304 ± 2	17.79 ± 0.41	28.1	0.1	157.1	41.1	0.037
48	PGC1199471	226.38255	1.58772	E — dE,N	919 ± 41	18.15 ± 0.46	17.3	0.1	126.1	56.6	NA
49	PGC1190714	226.40715	1.30309	E? — E/dE	2074 ± 17	17.43 ± 0.37	22.3	0.06	114.1	30	0.037
50	PGC1209872	226.46055	1.90834	E — dE	1721 ± 9	16.93 ± 0.31	29.4	0.11	177.2	61.1	0.032
51	PGC1213020	226.47165	2.00775	I — dI	1300 ± 31	18.35 ± 0.46	21.3	0.27	143.9	67.4	0.032
52	NGC5845	226.50330	1.63397	E — E	1450 ± 9	13.44 ± 0.15	60	0.15	152.9	72	0.034
53	PGC1218738	226.51410	2.18486	Sm — Sm	1659 ± 4	16.34 ± 0.31	41.5	0.06	148.4	32.6	0.030
54	PGC1191322	226.52805	1.32242	E? — E/dE	2300 ± 14	18.01 ± 0.34	19.4	0.21	66	53.5	0.032
55	PGC1215798	226.54695	2.09585	Scd — Scd	1824 ± 1	17.64 ± 1.92	51.1	0.68	5.2	82	0.030
56	NGC5846	226.62180	1.60629	E — E	1750 ± 32	11.09 ± 0.16	255.9	0.02	-	25	0.035
57	NGC5846A	226.62150	1.59494	E — E	2251 ± 18	12.72 ± 0.35	189.7	0.15	111.7	66.7	0.035
58	SDSSJ150634.25+001255.6	226.64265	0.21556	E? — ...	2006 ± 75	17.87 ± 0.5	28.7	0.21	22.5	53.3	0.035
59	PGC3119319	226.64265	1.55883	E — E	1509 ± 2	16.13 ± 0.35	-	-	140	-	0.035
60	NGC5841	226.64580	2.00488	S0-a — S0	1257 ± 2	14.55 ± 0.34	70.5	0.39	152.9	90	0.030

<sup>a</sup>data from HYPERLEDA <http://leda.univ-lyon1.fr> (Makarov et al. 2014). <sup>b</sup>data from Mahdavi et al. (2005).

has an average apparent B magnitude of  $\langle B_T \rangle \sim 11.64 \pm 2.07$  mag. According to the HYPERLEDA classification, the group is dominated by ETGs, whose percentage achieves  $\sim 70$  per cent, similar to that in clusters. We further include as group members all the galaxies in the HYPERLEDA catalogue with a heliocentric radial velocity within  $\pm 3\sigma$  the group average velocity,  $\langle V_{hel} \rangle$ , and within a diameter of  $\sim 1.5$  Mpc around the centre of the group given by Ramella et al. (2002). Table 1 lists the properties of the 90 galaxies selected using

the method described above. Columns from 1 to 12 provide our ID member number, the galaxy name, J2000 coordinates, morphological type, heliocentric velocity, B total apparent magnitude, major axis diameter,  $D_{25}$ , axial ratio, position angle, inclination and the foreground galactic extinction, respectively. The morphological classification is taken from HYPERLEDA. This catalogue associates a type, T, to the morphological classification. Galaxies with  $T \leq 0$  are considered early-type. Ellipticals are in the range  $-5 \leq T \leq -3$ , Spirals have  $T \geq 0$ . Dwarf galaxies are not fully considered

**Table 1.** continued.

Id. Nr.	Galaxy	RA (J2000) [deg]	Dec. (J2000) [deg]	Morph. type [ <sup>a</sup> — <sup>b</sup> ]	Mean Hel. Vel [km/s]	$B_T$ [mag]	$D_{25}$ ['']	$\log r_{25}$	P.A. [deg]	Incl. [deg]	$E(B-V)$ [mag]
61	PGC1156476	226.67070	0.07675	E? — ...	1663 ± 11	18.07 ± 0.32	20.8	0.23	8.9	54.7	0.034
62	PGC1171244	226.67520	0.63445	E — dE	2260 ± 9	17.99 ± 0.28	18.1	0.18	169.7	90	0.033
63	NGC5846:[MTT2005]226	226.74300	1.99454	E — dE	1307 ± 60	-	-	-	-	-	0.030
64	NGC5850	226.78185	1.54465	Sb — Sb	2547 ± 3	11.89 ± 0.24	198.7	0.15	114.4	46.9	0.035
65	PGC1185172	226.89225	1.12043	S? — E/dE	1586 ± 8	17.64 ± 0.37	19.9	0.16	124	47.7	0.032
66	PGC054004	226.90500	2.01954	E — dE,N	1923 ± 10	15.86 ± 0.28	41.5	0.08	-	50.4	0.029
67	NGC5854	226.94880	2.5686	S0-a — S0	1730 ± 26	12.65 ± 0.09	181.2	0.63	55	90	0.028
68	PGC054016	226.94910	1.29209	E — E	2070 ± 7	15.67 ± 0.4	36.1	0.02	-	23.7	0.035
69	PGC1217593	227.00580	2.15102	E — E	1073 ± 24	18.04 ± 0.4	19.0	0.15	36.5	76.9	0.027
70	PGC054037	227.02335	1.65156	S? — S0/a	1843 ± 3	16.08 ± 0.73	34.5	0.29	115	63.4	0.032
71	NGC5846:[MTT2005]258	227.03550	2.90502	E — dE, N	1652 ± 60	-	-	-	-	-	0.027
72	NGC5846:[MTT2005]259	227.03835	1.42058	E — dE, N	2314 ± 60	-	-	-	-	-	0.032
73	PGC054045	227.03850	1.60856	I — dI	2158 ± 21	16.09 ± 0.46	37.8	0.04	-	25.5	0.032
74	SDSSJ150812.35+012959.7	227.05155	1.49975	E — dE,N	1537 ± 28	18.02 ± 0.36	22.3	0.01	-	16.6	0.032
75	NGC5846:[MTT2005]264	227.08275	1.68963	E — dE,N	2088 ± 60	-	-	-	-	-	0.029
76	PGC1206166	227.09445	1.79848	E — dE, N	1741 ± 13	18.08 ± 0.4	25.6	0.39	139.4	90	0.030
77	NGC5846:[MTT2005]268	227.10690	1.70693	E — dE	2049 ± 60	-	-	-	-	-	0.030
78	PGC1209573	227.19660	1.9001	E — dE	1991 ± 8	16.67 ± 0.3	41.1	0.36	159.6	90	0.020
79	PGC1176385	227.26785	0.82193	Sa — S0/a	1644 ± 2	16.81 ± 0.29	33.7	0.22	179	57.9	0.033
80	SDSSJ150907.83+004329.7	227.28270	0.72479	E — dE	1666 ± 10	17.69 ± 0.35	43.5	0.49	133.8	90	0.032
81	PGC1210284	227.31225	1.92142	E — dE	1728 ± 9	16.64 ± 0.29	34.5	0.2	87.2	90	0.020
82	NGC5864	227.38995	3.05272	S0 — S0	1802 ± 21	12.70 ± 0.19	150.7	0.51	66.5	90	0.027
83	NGC5869	227.45580	0.47011	S0 — ...	2074 ± 16	13.15 ± 0.25	131.3	0.19	110.7	61.5	0.032
84	UGC09746	227.57010	1.93358	Sbc — Scd	1736 ± 4	14.84 ± 0.27	46.7	0.53	138.6	78.6	0.020
85	UGC09751	227.74365	1.43753	Sc — Sd	1553 ± 7	15.97 ± 0.67	73.8	0.58	118.5	78.8	0.027
86	PGC1202458	227.75550	1.6806	E — dE	1652 ± 18	17.28 ± 0.29	27.4	0.09	171.9	53.1	0.024
87	SDSSJ151121.37+013639.5	227.83965	1.61079	E — dE	2029 ± 69	-	-	-	-	-	0.024
88	UGC09760	228.01050	1.69849	Scd — Sd	2021 ± 3	15.20 ± 0.65	106.7	0.73	61.2	85.1	0.025
89	PGC1199418	228.03420	1.58584	E — E	1941 ± 3	17.00 ± 0.33	20.3	0.07	137.7	45.4	0.025
90	PGC1215336	228.10005	2.07999	S? — ...	1684 ± 10	16.94 ± 0.29	30.1	0.19	96.9	50.9	0.015

in this classification. However, Sm, magellanic Irr, ( $T=9$ ) and generic Irr ( $T=10$ ) are dwarfs. Dwarf early-type are not classified in the HYPERLEDA scheme. We adopt for them the same classification scheme and values of  $T$  as for bright ones. We also added in column 5 the morphological type provided by Mahdavi et al. (2005). These authors identified dwarfs among Ellipticals (Es) distinguishing normal dEs and nucleated dEs,N. Apart from luminosity classification, in very few cases the two morphological classifications differ. Figure 1 shows the morphological type distribution (top panel) and the apparent B-band magnitudes (bottom panel) of the 90 members of the group. Members with morphological type  $T \leq -4$  and apparent B magnitudes  $\geq 16$  dominate.

We compared the members of the group by HYPERLEDA and Mahdavi et al. (2005) selection criteria with those identified in the literature. Mahdavi et al. (2005) argue, on statistical grounds, that a total of  $251 \pm 10$  galaxies, listed in their Table 1 composed of 324 candidates, are members of the group. In their Table 2 Mahdavi et al. (2005) provide the number of spectroscopically confirmed members, which amount to 84, belonging to different classes statistically established. These classes range from 0 to 5, i.e from members confirmed by spectroscopy, priority rating 0, to galaxies excluded by their statistical surface brightness criteria, priority rating 5. Our selection of 90 members includes all 84 spectroscopically confirmed members of Mahdavi et al. (2005), four dwarfs with spectroscopic redshift included in the Eigenthaler & Zeilinger (2010) list, plus other two ETGs in HYPERLEDA. We report in col. 3 of Table 3 the identification number provided by Mahdavi et al. (2005) and by Eigenthaler & Zeilinger (2010). All dwarfs in the Eigenthaler & Zeilinger (2010) list, but two, NGC 5486-56

and NGC 5846-51, are included by our selection criteria. PGC087108 according to Eigenthaler & Zeilinger (2010) are two HII regions classified as individual galaxies in SDSS e in PGC. UV imaging indicated that it is a galaxy (see Section 4.1).

Summarizing, our selection procedure includes all spectroscopically confirmed members present in the Mahdavi et al. (2005) and Eigenthaler & Zeilinger (2010) lists within a diameter of  $\sim 1.5$  Mpc about the group centre. As explained in the following section we extended the search of spectroscopic possible members in a wider area of 4 Mpc. Additional galaxies, not included in Mahdavi et al. (2005) and Eigenthaler & Zeilinger (2010), with a redshift measure are listed in Table B1. Although compatible with membership in the redshift space, they are distant from the centre of mass of the group and outside the box of 1.8 Mpc considered by Mahdavi et al. (2005).

## 2.2 Substructures

The presence of substructures in a galaxy group is a signature of recent accretion and therefore probes the evolution of its members (e.g Firth et al. 2006; Hou et al. 2012). Substructures manifest as a deviation in the spatial and/or velocity arrangement of the system.

If a group is a dynamically relaxed system, the spatial distribution of its galaxies should be approximately spherical and their velocity distribution Gaussian. The presence of substructures indicates a departure from this quasi-equilibrium state. As already discussed in Paper II, at least one of the following characteristics shows the presence of sub-

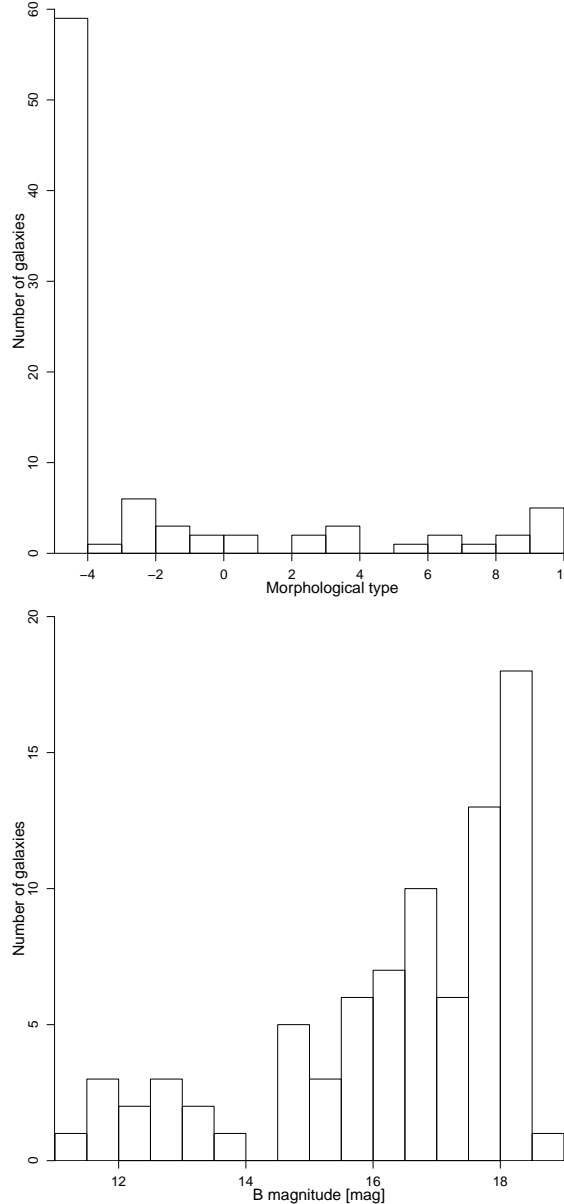


**Figure 1.** Morphological type (top) and B magnitude (bottom) distributions of NGC 5846 members from HYPERLEDA. All members are spectroscopically confirmed (see Section 2).

structures: (i) significant multiple peaks in the galaxy position distribution; (ii) significant departures from a single-Gaussian velocity distribution; (iii) correlated deviations from the global velocity and position distribution.

Fig. 2 shows the projected spatial distribution of the group members (top panel). Galaxies are separated in B magnitude bins and morphological types. ETGs, Spirals and Irregulars, with absolute magnitudes  $M_B > -16$  and,  $M_B < -16$  are indicated with squares, triangles and circles of increasing size, respectively. The group is dominated by ETGs (72 per cent), 60 per cent Ellipticals<sup>1</sup> approximately homogeneously distributed. Two peaks may be present in the projected spatial distribution.

The velocity distribution of group members is shown

<sup>1</sup> Morphological type  $\leq -3$

in Figure 2 (bottom panel, filled bins). To discern if the heliocentric radial velocity has a Gaussian distribution, we applied the Anderson-Darling normality test and found it does not significantly depart ( $p$ -value = 0.92) from normality.

We also performed the Dressler & Shectman (1988) test (DS test hereafter), which uses both spatial information and velocity, to find substructures in our group. The DS test identifies a fixed number, NN, of nearest neighbours on the sky around each galaxy, computes the local mean velocity and velocity dispersion of this subsample, and compares these values with the average velocity and velocity dispersion of the entire group,  $\bar{v}$  and  $\sigma_{gr}$  respectively. The deviations of the local average velocity and the dispersions from the global values are summed. In particular, for the galaxy  $i$ , the deviation of its projected neighbors is defined as  $\delta_i = (NN + 1)/\sigma_{gr} [ (v_{loc} - \bar{v})^2 + (\sigma_{loc} - \sigma)^2 ]$ , where  $v_{loc}$  and  $\sigma_{loc}$  are the local average velocity and velocity dispersion. The total deviation,  $\Delta$ , is the sum of the local deviations,  $\delta_i : \Delta = \sum_i^N \delta_i$ , where  $N$  is the number of the group members. If the group velocity distribution is close to Gaussian and the local variations are only random fluctuations,  $\Delta$  will be of the order  $N$ . If  $\Delta$  varies significantly from  $N$  there is probable substructure.

To compute  $\delta$ , we set the number of neighbors, NN, at  $10 \approx N^{1/2}$  (see e.g. Silverman 1986). Since  $\delta_i$  are not statistically independent it is necessary to calibrate the  $\Delta$  statistic by performing a Monte Carlo analysis. The velocities are randomly shuffled among the positions and  $\Delta_{sim}$  is recomputed 10000 times to provide the probability that the measured  $\Delta$  is a random result. The significance of having substructure, given by the  $p$ -value, is quantified by the ratio of the number of the simulations in which the value of  $\Delta_{sim}$  is larger than the observed value, and the total number of simulations:  $p = (N(\Delta_{sim} > \Delta)/N_{sim})$ .

It should be noted that the  $\Delta$  statistic is insensitive to subgroups that are well superimposed. It relies on some displacement of the centroids of the subgroups.

The  $p$ -value measures the probability that a value of  $\Delta_{sim} \geq \Delta$  occurs by chance; a  $p$ -value  $> 0.10$  gives a high significance level to the presence of substructures, values ranging from 0.01 and 0.10 give substructures from marginal to probable.

In Figure 3, we show the Dressler-Shectman ‘bubble-plot’; each galaxy in the group is marked by a circle whose diameter scales with  $e^\delta$ . Larger circles indicate larger deviations in the local kinematics compared to the global one. Many large circles in an area indicate a correlated spatial and kinematical variation, i.e. a substructure. We also show the position of NGC 5846 and NGC 5813. The group does not present significant substructures ( $p = 0.07$ ).

### 2.3 Group’s environment density analysis

In order to characterize the environment of the group, we have considered the galaxy distribution within a box of  $4 \times 4$  Mpc<sup>2</sup> (about two times the size of a typical group) centred on NGC 5846. From the HYPERLEDA database we have selected all the galaxies within such box with a heliocentric radial velocity within  $\pm 3\sigma$  of the group mean velocity, as given in the catalog of Ramella et al. (2002). We have found

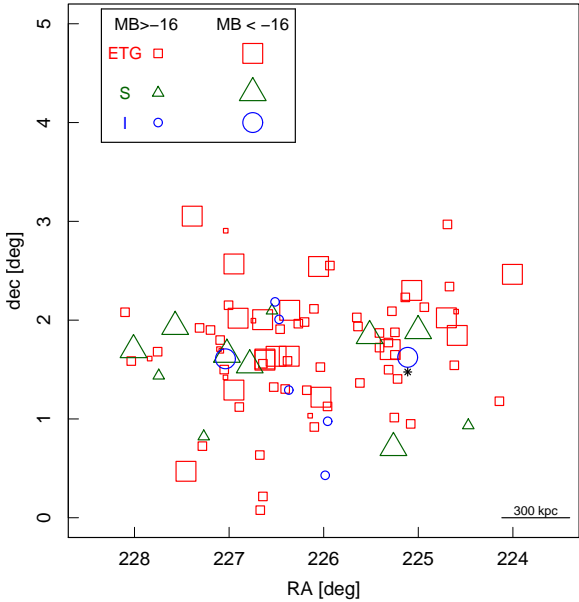


**Figure 2.** *Top:* Spatial distribution of galaxy members separated in B magnitude bins and morphological type. The smallest symbols are galaxies with no B magnitudes. Black asterisk refer to galaxies with no B magnitudes and no morphological types. *Bottom:* Histogram of the heliocentric radial velocity ( $10-3000 \text{ km s}^{-1}$ ) of galaxies within a box of  $4 \text{ Mpc}^2$  centred on NGC 5846. The width of the velocity bins is  $100 \text{ km s}^{-1}$ . Green filled bins show the velocity distribution of the 90 members listed in Table 1.

136 galaxies (Table 1 and Table B1 in Appendix B). In the bottom panel of Figure 2, we highlight the velocity distribution of group members (green filled bins) given in Table 1 superposed on that of galaxies in the  $4 \times 4 \text{ Mpc}^2$  box. Among these galaxies, we have selected only those more luminous than 15.5 mag in the B band (i.e. the magnitude limit of the galaxies in Ramella et al. (2002), and on this sample we performed a density analysis. The 2D binned kernel-smoothed number density contour map is shown in

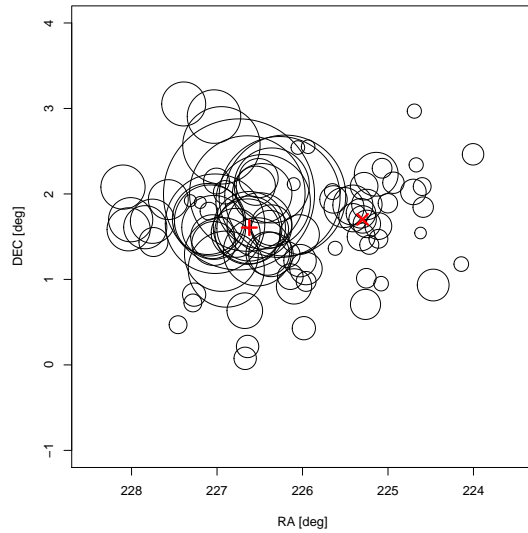


**Figure 3.** Dressler & Shectman (1988) ‘bubble-plot’ based on the ten nearest galaxies. The bubble size is proportional to the squared deviation of the local velocity distribution from the group velocity distribution. Red plus and cross show the position of NGC 5846 and NGC 5813 respectively.

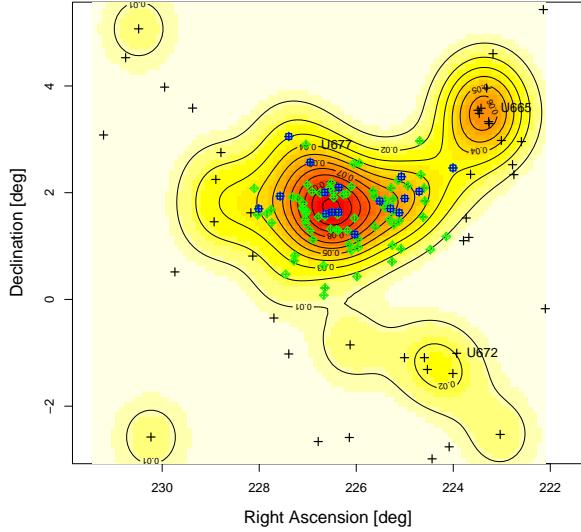


**Figure 4.** Spatial distribution of galaxies within a box of  $4 \times 4 \text{ Mpc}^2$  centred on NGC 5846 (shaded yellow/red area). Blue squares show the members of the group listed in the catalogue of Ramella et al. (2002) and green diamonds indicate the added members (Section 2). The map is normalized to the total density. The 2D binned kernel-smoothed number density contours for the galaxies with  $m_B \leq 15.5 \text{ mag}$  (circle + cross) are shown. The value of  $m_B = 15.5 \text{ mag}$  is the magnitude limit of the Ramella et al. (2002) catalogue.

Figure 4. Density in the  $4 \times 4 \text{ Mpc}^2$  box (shaded yellow) is colour coded. The highest densities correspond to the red regions; in the normalized map, density levels above 0.05 are in yellow. Blue squares show the members of the group from the catalogue of Ramella et al. (2002) and green diamonds indicate the new members that we have added (as explained in Section 2.1).

A high density region approximately centred on NGC 5846, and elongated towards NGC 5813, the second B-band brighter member, appears. There are also two poor groups, USGC U665 and USGC U672, likely falling toward NGC 5846.

#### 2.4 Group dynamical properties

The virial theorem provides the standard method to estimate the mass of a self-gravitating system from dynamical parameters, positions and velocities of the group members. It applies if the system analyzed is in dynamical equilibrium and its luminosity is a tracer of the mass.

We derived the kinematic and dynamical properties of NGC 5846, following the approach described in Firth et al. (2006, their Table 6) and already used in Marino et al. (2010) for LGG 225 and Marino et al. (2014) for USGC U268 and USGC U376.

Results are summarized in Table 2. The errors have been computed via jackknife simulations (e.g. Efron 1982). In order to obtain an estimate of the compactness of the group, we computed the harmonic mean radius using the projected separations  $r_{ij}$  between the  $i$ -th and  $j$ -th group member. Figure 5 shows the relative positions of the group members with superposed a circle centred on the centre of mass of the group and radius corresponding to the virial radius.

The projected mass is about two times the virial mass. The contribution of the 30 galaxies surrounding NGC 5813 (Table 1) is about 20 per cent of the virial mass and 34% of the projected one (see the second line in Table 2). For comparison, the projected mass of the groups USGC 268 and USGC U376 (Marino et al. 2014), is a factor 3-4 times the virial one. Using N-body simulations, Perea et al. (1990) showed that the virial mass estimate is better than the projected mass estimate since it is less sensitive to anisotropies or sub-clustering. However, it may be affected by the presence of interlopers, i.e. unbound galaxies, and by a mass spectrum. Both factors would cause an overestimation of the group mass. Therefore the estimated masses are upper limits. Another caveat concerning the virial mass is that the groups may not be virialized (e.g. Ferguson & Sandage 1990).

The larger difference in the virial and projected mass estimates of USGC U268 and USGC U376 may suggest a larger probability of interlopers, although these groups are, on average, closer than NGC5846 group (15 and 19 Mpc respectively Marino et al. 2014), or that these are not yet virialized.

The crossing time is usually compared to the Hubble time to determine whether the groups are gravitationally bound systems. The derived crossing time of NGC 5846 group (see Table 2) suggests that it could be virialized (e.g. Firth et al. 2006).

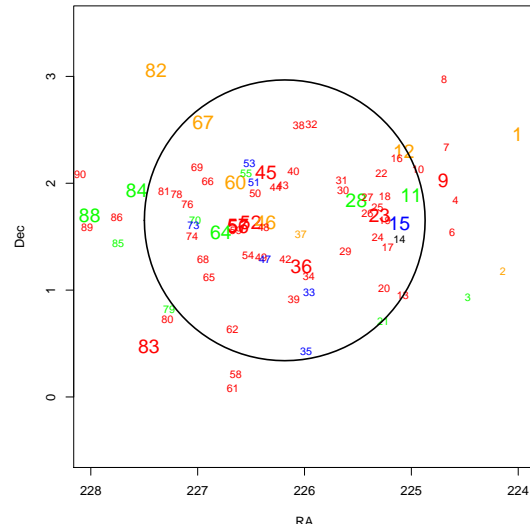


**Table 2.** Kinematical and dynamical properties of NGC 5846

Group name	Center of mass RA [deg]	Center of mass Dec	$V_{group}$ [km/s]	Velocity dispersion [km/s]	D [Mpc]	Harmonic radius [Mpc]	Virial mass [ $10^{13} M_{\odot}$ ]	Projected mass [ $10^{13} M_{\odot}$ ]	Crossing time $\times H_0$
NGC 5846	226.18501	1.65321	$1798^{+8}_{-10}$	$327^{+12}_{-2}$	$24.0^{+0.1}_{-0.1}$	$0.35^{+0.01}_{-0.01}$	$4.15^{+0.24}_{-0.16}$	$8.24^{+0.56}_{-0.13}$	$0.12^{+0.00}_{-0.01}$
NGC5846 <sup>1</sup>	226.76139	1.65059	$1800^{+13}_{-15}$	$332^{+18}_{-3}$	$24.0^{+0.2}_{-0.2}$	$0.27^{+0.01}_{-0.01}$	$3.24^{+0.29}_{-0.20}$	$5.42^{+0.43}_{-0.13}$	$0.09^{+0.01}_{-0.00}$

<sup>1</sup> The same quantities computed excluding the first thirty galaxies in Table 1, i.e., NGC 5813 and its surroundings.

### 3.2 Aperture photometry

UV and optical magnitudes of the brighter members ( $B_T \leq 15.5$  mag) have been obtained as follows.

The UV and optical surface photometry was carried out using the ELLIPSE fitting routine in the STSDAS package of IRAF (Jedrzejewski 1987). The SDSS images (corrected frames with the soft bias of 1000 counts subtracted) in the five bands were registered to the corresponding *GALEX* NUV intensity images before evaluating brightness profiles, using the IRAF tool register. We masked the foreground stars and the background galaxies in the regions where we measured the surface brightness profiles. To secure a reliable background measure, we forced the measure of 5 isophotes well beyond the galaxy emission.

From the surface brightness profiles, we derived total apparent magnitudes as follows. For each profile, we computed the integrated apparent magnitude within elliptical isophotes up to the radius where the mean isophotal intensity is  $2\sigma$  above the background. The background was computed around each source, as the mean of sky value of the outer five isophotes. Errors of the UV and optical magnitudes were estimated by propagating the statistical errors on the mean isophotal intensity provided by ELLIPSE. In addition to the statistical error, we added systematic uncertainties in the zero-point calibration of 0.05 and 0.03 mag in FUV and NUV respectively (Morrissey et al. 2007). Surface photometry was corrected for galactic extinction assuming Milky Way dust properties with  $R_V=3.1$  (Cardelli et al. 1989),  $A_{FUV}/E(B-V) = 8.376$ ,  $A_{NUV}/E(B-V) = 8.741$ , and  $A_r/E(B-V) = 2.751$ .

Table 4 lists the measured AB magnitudes both in UV and optical<sup>2</sup> bands., uncorrected for foreground Galaxy extinction. UV and optical magnitudes of fainter members were extracted from the *GALEX* and SDSS pipelines. We used the FUV and NUV calibrated magnitudes and the Model magnitudes<sup>3</sup> from the *GALEX* and SDSS pipelines, respectively.

## 4 RESULTS

Hereafter, following the definition of Tammann (1994), we considered as dwarfs galaxies fainter than  $M_B = -16$  mag ( $M_V = -17$  mag), and as ETGs, galaxies with morphological type  $T \leq 0$  (i.e E-S0a-dE-dE,N-dS0) as in Boselli & Gavazzi (2014).

<sup>2</sup> We converted SDSS counts to magnitudes following the recipe provided in <http://www.sdss.org/dr7/algorithms/fluxcal.html>.

<sup>3</sup> <http://www.sdss.org/dr5/algorithms/photometry.html>

### 4.1 UV vs. optical morphological classification

Table 1 (column 5) compares the morphological classification of members we adopted with that in Mahdavi et al. (2005). In Appendix A we show the UV (left panels) and SDSS (right panels) colour composite images of all 90 galaxy members. The HYPERLEDA optical morphological classification is in good agreement with that suggested by UV images.

Here we present the galaxies of the group for which UV images suggest a different morphological classification.

ID 15: NGC 5811 is a blue UV galaxy with a bar, visible both in optical and UV, representing the main body of the galaxy. It is a late type galaxy, SBm, rather than dE.

ID 20: SDSSJ150100.85+010049.8, we adopted the HYPERLEDA classification.

ID 28: UGC09661 shows a blue bar in UV, the SBd classification seems more appropriate than Sdm.

ID 35: PGC087108, shows two distinct bright sources in a common blue envelope in the UV image. It is classified as Irregular; the classification seems correct.

ID 47: PGC1190358 morphology is quite irregular in the UV image. It does not appear a dE as in Mahdavi et al. (2005).

ID 53: PGC 1218738 seems to have a blue inner bar in the UV image although it is classified Sm.

ID 55: PGC1215798, classified Scd, shows peculiar tidal tails, that we consider as possible interaction signatures.

ID 58: SDSSJ150634.25+001255.6. We consider this galaxy a dE ( $T=5\pm 5$ ) as in HYPERLEDA.

ID 60: NGC 5841 is a S0-a, incipient arms are visible in the SDSS image. The UV composite image shows that the colour is consistent with a old stellar population.

ID 64: NGC5850 is a barred Spiral with a ring and irregular spiral arms, likely signatures of interaction. The irregular arms are markedly extended in the UV image much further out than the optical size. We suggest a classification of SB(r)b as in RC3.

ID 65: PGC1185172 is classified S? ( $T=10\pm 5$ ). We adopted the dE classification of Mahdavi et al. (2005).

ID 67: NGC 5854 is classified S0-a in HYPERLEDA and S0 in Mahdavi et al. (2005). The UV image suggests the presence of incipient arms, more consistent with the HYPERLEDA classification.

ID 70: PGC054037 is classified S? in HYPERLEDA ( $T=1\pm 5$ ) and S0a in Mahdavi et al. (2005). We adopt this latter classification.

ID 80: PGC4005496 appears quite blue in UV composite image and with an irregular shape. Rather than a E/dE classification we suggest Im.

ID 88: UGC09760, seen edge-on, is classified Scd/Sd. The yellow spot on the blue galaxy disk of the UV image is

**Table 3.** The NGC 5846 group members and the journal of the UV observations with *GALEX*.

Id Nr.	Galaxy	MTT05	P	NUV	FUV	Survey
				Exp. Time [sec])	Exp. Time [sec]	
1	PGC053384	...	...	1602.1	1602.1	MIS
2	PGC1186917	...	...	1640.7	1640.7	MIS
3	PGC1179522	009	0	1640.7	1640.7	MIS
4	PGC184851	013	2	1648.0	162.0	G16 AIS
5	SDSS J145824.22+020511.0	014	1	1648.0	162.0	G16 AIS
6	SDSS J145828.64+013234.6	017	2	1640.7	1640.7	MIS
7	PGC1223766	018	3	1648.0	162.0	G16 AIS
8	PGC1242097	020	5	2107.5	2107.5	MIS
9	PGC053521	021	0	1648.0	162.0	G16 AIS
10	SDSS J145944.77+020752.1	030	2	1648.0	162.0	G16 AIS
11	NGC5806	037	0	2521.2	2521.2	G13
12	PGC053587	042	0	1648.0	162.0	G16 AIS
13	SDSS J150019.17+005700.3	045	1	335.0	159.0	AIS
14	NGC 5846:[MTT2005] 046	046	0	2521.2	2521.2	G13
15	NGC5811	047	3	2521.2	2521.2	G13
16	SDSS J150033.02+021349.1	048	1	1648.0	162.0	G16 AIS
17	PGC1193898	055	2	2521.2	2521.2	G13
18	SDSS J150059.35+015236.1	058	2	2521.2	2521.2	G13
19	SDSS J150059.35+013857.0	059	5	2521.2	2521.2	G13
20	SDSS J150100.85+010049.8	060	2	335.0	159.0	AIS
21	PGC053636 <sup>a</sup>	061	0			
22	SDSS J150106.96+020525.1	063	2	2521.2	2521.2	G13
23	NGC5813	064	0	2521.2	2521.2	G13
24	PGC1196740	068	2	2521.2	2521.2	G13
25	PGC1205406	069	3	2521.2	2521.2	G13
26	SDSS J150138.39+014319.8	073	2	2521.2	2521.2	G13
27	PGC1208589	075	3	2521.2	2521.2	G13
28	UGC09661	083	0	2521.2	2521.2	G13
29	PGC1192611	088	3	5299.3	2359.1	G11
30	SDSS J150233.03+015608.3	090	1	2521.2	2521.2	G13
31	SDSS J150236.05+020139.6	091	3	2521.2	2521.2	G13
32	PGC1230503	113	3	2399.4	2399.4	MIS
33	SDSS J150349.93+005831.7	114	0	5299.3	2359.1	G11
34	PGC1185375	115	0	5299.3	2359.1	G11
35	PGC087108	NGC5846 41/42	Eigenthaler	1692.0	1692.0	MIS
36	NGC5831	122	0	5299.3	2359.1	G11
37	PGC1197513	124	0	5299.3	2359.1	G11
38	PGC1230189	125	3	2399.4	2399.4	MIS
39	PGC1179083	131	2	5299.3	2359.1	G11
40	PGC1216386	132	3	2399.4	2399.4	MIS
41	SDSS J150434.31+010156.9	139	1	5299.3	2359.1	G11
42	PGC1190315	142	0	5299.3	2359.1	G11
43	SDSS J150448.49+015851.3	144	2	2399.4	2399.4	MIS
44	PGC1211621	148	0	2399.4	2399.4	MIS
45	NGC5838	159	0	2399.4	2399.4	MIS
46	NGC5839	160	0	2484.2	2484.2	MIS
47	PGC1190358	162	0	5299.3	2359.1	G11
48	PGC1199471	165	3	2484.2	2484.2	MIS
49	PGC1190714	167	0	2484.2	2484.2	MIS
50	PGC1209872	177	0	1466.0	1466.0	G13
51	PGC1213020	180	3	1466.0	1466.0	G13
52	NGC5845	184	0	2484.2	2484.2	MIS
53	PGC1218738	187	2	1466.0	1466.0	G13
54	PGC1191322	191	0	2484.2	2484.2	MIS
55	PGC1215798	192	0	1466.0	1466.0	G13
56	NGC5846A	201	0	2484.2	2484.2	MIS
57	NGC5846	202	0	2484.2	2484.2	MIS
58	SDSS J150634.25+001255.6	NGC584644	Eigenthaler	1695.1	1694.1	MIS
59	PGC3119319	205	5	2484.2	2484.2	MIS
60	NGC5841	206	0	1466.0	1466.0	G13
61	PGC1156476	NGC584650	Eigenthaler	164.0	164.0	AIS
62	PGC1171244	212	3	1695.1	1694.1	MIS
63	SDSS J150658.37+015939.5	226	2	1466.0	1466.0	G13
64	NGC5850	233	0	2484.2	2484.2	MIS
65	PGC054004	241	3	163.0	163.0	AIS
66	PGC054004	244	0	2376.0	2375.0	MIS
67	NGC5854	246	0	2376.0	2375.0	MIS
68	PGC054016 <sup>a</sup>	247	0			
69	PGC1217593	252	5	2376.0	2375.0	MIS
70	PGC054037 <sup>b</sup>	256	4			
71	SDSS J150808.43+025416.5	258	3	2376.0	2375.0	MIS
72	NGC5846:[MTT2005]259 <sup>b</sup>	259	3			
73	PGC054045 <sup>b</sup>	260	0			
74	SDSS J150812.35+012959.7 <sup>b</sup>	261	3			
75	NGC 5846:[MTT2005] <sup>b</sup>	264	2			
76	PGC1206166 <sup>b</sup>	266	2			
77	SDSS J150825.57+014224.8 <sup>b</sup>	268	2	...		
78	PGC1209573 <sup>a</sup>	276	3			
79	PGC1176385	283	0	1696.0	1696.0	MIS
80	SDSS J150907.83+004329.7	287	2	1696.0	1696.0	MIS
81	PGC1210284 <sup>a</sup>	290	3			
82	NGC5864	299	0			
83	NGC5869	NGC5869	Eigenthaler	1450.6	1450.6	MIS
84	UGC09746	305	0	1655.0	<sup>a</sup>	G16
85	UGC09751	311	0	1696.0	1696	MIS
86	PGC1202458	313	2	1655.0	<sup>a</sup>	G16
87	SDSS J151121.37+013639.5	317	1	1655.0	<sup>b</sup>	G16
88	UGC09760	321	0	1655.0	111.0	G16 AIS
89	PGC1199418	323	5	1655.0	<sup>a</sup>	G16
90	PGC1215336	NGC584652	Eigenthaler	2905.9	1732.3	MIS

Notes. – Col. 1 and col. 2: galaxy identification; col. 3 and col. 4 galaxy identification and membership probability in Mahdavi et al. (2005) Table 1, respectively. P values are: 0, no-SDSS spectroscopic redshift; 1, probable member; 2, possible member; 3, conceivable member; 4 and 5 likely not a member. <sup>a</sup> The UV images have a distance from the center of the field of view >50'. <sup>b</sup> There are no FUV GALEX images for these galaxies.

**Table 4.** UV and optical photometry of the galaxy group.

Id. Nr.	Galaxy	FUV [AB mag]	NUV [AB mag]	u [AB mag]	g [AB mag]	r [AB mag]	i [AB mag]	z [AB mag]
1	PGC053384	20.520 ± 0.090	18.740 ± 0.040	16.250 ± 0.010	14.670 ± 0.010	14.080 ± 0.010	13.7501 ± 0.010	13.700 ± 0.010
2	PGC1186917	23.678 ± 0.405	21.039 ± 0.100	18.449 ± 0.058	16.911 ± 0.006	16.236 ± 0.005	15.901 ± 0.005	15.684 ± 0.014
3	PGC1179522	21.368 ± 0.113	20.067 ± 0.062	17.991 ± 0.040	16.470 ± 0.006	15.761 ± 0.005	15.453 ± 0.006	15.235 ± 0.014
4	PGC184851	21.851 ± 0.370	19.926 ± 0.115	17.431 ± 0.025	15.806 ± 0.003	15.040 ± 0.003	14.670 ± 0.003	14.362 ± 0.009
5	SDSSJ145824.22+020511.0	21.629 ± 0.220	20.339 ± 0.482	18.913 ± 0.046	17.397 ± 0.012	16.751 ± 0.010	16.446 ± 0.011	16.238 ± 0.038
6	SDSSJ145828.64+013234.6	20.617 ± 0.090	19.668 ± 0.048	19.227 ± 0.165	17.886 ± 0.015	17.201 ± 0.012	16.885 ± 0.015	16.848 ± 0.064
7	PGC1223766	21.924 ± 0.292	19.372 ± 0.131	17.886 ± 0.015	16.769 ± 0.003	15.372 ± 0.003	15.159 ± 0.003	15.018 ± 0.006
8	PGC1242097	18.504 ± 0.013	17.970 ± 0.009	16.796 ± 0.010	15.769 ± 0.003	14.330 ± 0.010	13.620 ± 0.010	13.220 ± 0.010
9	PGC053521	18.900 ± 0.040	15.920 ± 0.010	14.330 ± 0.010	13.620 ± 0.010	13.220 ± 0.010	13.080 ± 0.010	13.080 ± 0.010
10	SDSSJ145944.77+020752.1	21.650 ± 0.273	19.271 ± 0.139	18.114 ± 0.018	17.519 ± 0.017	17.193 ± 0.022	17.113 ± 0.096	17.113 ± 0.096
11	NGC5806	15.830 ± 0.050	15.180 ± 0.030	13.600 ± 0.010	11.990 ± 0.010	11.320 ± 0.010	10.860 ± 0.010	10.600 ± 0.010
12	PGC053587	19.240 ± 0.040	16.870 ± 0.010	15.140 ± 0.010	14.440 ± 0.010	14.020 ± 0.010	13.950 ± 0.010	13.950 ± 0.010
13	SDSSJ150019.17+005700.3	21.101 ± 0.267	18.957 ± 0.113	17.303 ± 0.010	16.597 ± 0.009	16.306 ± 0.010	16.158 ± 0.031	16.158 ± 0.031
14	NGC5846:[MTT2005]046	23.516 ± 0.354	23.311 ± 0.376					
15	NGC5811	17.310 ± 0.050	16.780 ± 0.030	15.620 ± 0.010	14.450 ± 0.010	13.810 ± 0.010	13.350 ± 0.010	13.400 ± 0.010
16	SDSSJ150033.02+021349.1	21.365 ± 0.269	18.510 ± 0.098	16.979 ± 0.009	16.306 ± 0.008	16.038 ± 0.011	16.588 ± 0.089	16.588 ± 0.089
17	PGC1193898	20.438 ± 0.093	18.004 ± 0.061	16.410 ± 0.006	15.691 ± 0.005	15.339 ± 0.006	15.136 ± 0.022	15.136 ± 0.022
18	SDSSJ150509.35+015236.1	21.946 ± 0.186	19.614 ± 0.152	18.506 ± 0.022	17.840 ± 0.020	17.568 ± 0.026	17.496 ± 0.104	17.496 ± 0.104
19	SDSSJ150059.35+013857.0	23.147 ± 0.403	19.598 ± 0.189	17.968 ± 0.017	17.216 ± 0.015	16.814 ± 0.014	16.528 ± 0.043	16.528 ± 0.043
20	SDSSJ150100.85+010049.8	21.456 ± 0.333	20.303 ± 0.125	18.980 ± 0.110	17.800 ± 0.020	17.394 ± 0.018	17.487 ± 0.072	17.126 ± 0.093
21	PGC053636			16.888 ± 0.012	15.640 ± 0.003	15.004 ± 0.003	14.691 ± 0.003	14.460 ± 0.006
22	SDSSJ150106.96+020525.1	22.252 ± 0.198	19.840 ± 0.245	18.069 ± 0.020	17.350 ± 0.018	17.124 ± 0.020	16.935 ± 0.074	16.935 ± 0.074
23	NGC5813	17.910 ± 0.050	16.330 ± 0.030	13.320 ± 0.010	11.450 ± 0.010	10.500 ± 0.010	10.140 ± 0.010	9.880 ± 0.010
24	PGC1196740	20.898 ± 0.068	19.991 ± 0.049	18.531 ± 0.076	17.315 ± 0.010	16.851 ± 0.011	16.595 ± 0.013	16.473 ± 0.042
25	PGC1205406	22.333 ± 0.153	21.003 ± 0.110	18.954 ± 0.101	17.612 ± 0.013	17.006 ± 0.022	16.745 ± 0.026	16.678 ± 0.062
26	SDSSJ150138.39+014319.8	21.898 ± 0.262	19.030 ± 0.110	17.583 ± 0.012	16.877 ± 0.011	16.482 ± 0.012	16.589 ± 0.056	16.589 ± 0.056
27	PGC1208589	22.332 ± 0.136	21.662 ± 0.111	18.549 ± 0.085	17.259 ± 0.011	16.691 ± 0.011	16.429 ± 0.015	16.168 ± 0.045
28	UGC09661	16.690 ± 0.050	16.420 ± 0.030	15.190 ± 0.010	14.230 ± 0.010	14.040 ± 0.010	13.280 ± 0.010	13.670 ± 0.010
29	PGC1192611	21.618 ± 0.094	19.423 ± 0.149	17.909 ± 0.018	17.349 ± 0.021	17.103 ± 0.032	17.063 ± 0.116	17.063 ± 0.116
30	SDSSJ150233.03+015608.3	22.248 ± 0.141	21.389 ± 0.106	19.425 ± 0.209	17.918 ± 0.027	17.294 ± 0.021	17.074 ± 0.039	17.015 ± 0.096
31	SDSSJ150236.05+020139.6	21.659 ± 0.146	19.897 ± 0.205	17.854 ± 0.014	17.196 ± 0.016	16.876 ± 0.016	16.824 ± 0.052	16.824 ± 0.052
32	PGC1230503	23.826 ± 0.619		18.591 ± 0.076	17.157 ± 0.010	16.491 ± 0.007	16.202 ± 0.010	15.991 ± 0.027
33	SDSSJ150349.93+005831.7	18.110 ± 0.018	17.644 ± 0.007	17.938 ± 0.050	16.744 ± 0.009	16.430 ± 0.011	16.058 ± 0.012	15.805 ± 0.032
34	PGC1185375	23.627 ± 0.484	19.915 ± 0.050	17.670 ± 0.040	16.002 ± 0.004	15.247 ± 0.003	14.865 ± 0.004	14.598 ± 0.008
35	PGC087108	17.170 ± 0.013	17.073 ± 0.008	17.571 ± 0.041	16.622 ± 0.008	16.404 ± 0.010	16.449 ± 0.017	16.427 ± 0.052
36	NGC5831	18.900 ± 0.060	17.150 ± 0.030	14.070 ± 0.010	12.110 ± 0.010	11.300 ± 0.010	10.860 ± 0.010	10.630 ± 0.010
37	PGC1197513	19.675 ± 0.035	18.845 ± 0.014	17.190 ± 0.030	15.932 ± 0.004	15.413 ± 0.005	15.169 ± 0.006	15.052 ± 0.018
38	PGC1230189		19.916 ± 0.058	17.214 ± 0.032	15.565 ± 0.005	14.853 ± 0.004	14.473 ± 0.005	14.308 ± 0.014
39	PGC1179083	23.494 ± 0.506		19.196 ± 0.114	17.358 ± 0.011	16.680 ± 0.013	16.516 ± 0.017	16.409 ± 0.033
40	PGC1216386	23.282 ± 0.282	20.920 ± 0.099	18.466 ± 0.057	17.006 ± 0.007	16.362 ± 0.007	16.044 ± 0.007	15.828 ± 0.025
41	NGC5846:[MTT2005]139		22.596 ± 0.241	19.619 ± 0.149	18.534 ± 0.032	17.808 ± 0.022	17.564 ± 0.028	17.346 ± 0.085
42	PGC1190315		20.907 ± 0.068	18.222 ± 0.096	16.485 ± 0.006	15.775 ± 0.005	15.386 ± 0.008	15.207 ± 0.020
43	SDSSJ150448.49+015851.3	21.178 ± 0.085	20.263 ± 0.071	18.979 ± 0.126	17.818 ± 0.018	17.275 ± 0.021	17.098 ± 0.027	17.033 ± 0.089
44	PGC1211621	19.296 ± 0.028	18.954 ± 0.016	17.987 ± 0.031	17.110 ± 0.006	16.671 ± 0.007	16.545 ± 0.009	16.502 ± 0.032
45	NGC5838	18.290 ± 0.050	16.700 ± 0.030	13.320 ± 0.010	11.520 ± 0.010	10.710 ± 0.010	10.240 ± 0.010	9.980 ± 0.010
46	PGC1190358	19.420 ± 0.060	18.010 ± 0.030	14.620 ± 0.010	12.930 ± 0.010	12.100 ± 0.010	11.690 ± 0.010	11.400 ± 0.010
47	PGC1190358	19.199 ± 0.029	18.794 ± 0.013	18.308 ± 0.073	17.933 ± 0.018	17.612 ± 0.022	17.651 ± 0.038	18.249 ± 0.254
48	PGC1199471		21.734 ± 0.159	19.198 ± 0.124	17.612 ± 0.012	16.938 ± 0.012	16.641 ± 0.012	16.456 ± 0.074
49	PGC1190714	23.202 ± 0.302	20.520 ± 0.087	18.466 ± 0.063	17.004 ± 0.008	16.350 ± 0.006	16.018 ± 0.007	15.908 ± 0.024
50	PGC1209872	23.082 ± 0.399	21.006 ± 0.120	18.402 ± 0.076	16.593 ± 0.006	15.860 ± 0.005	15.518 ± 0.005	15.308 ± 0.019
51	PGC1213020	19.849 ± 0.053	19.574 ± 0.037	18.599 ± 0.074	17.817 ± 0.014	17.448 ± 0.025	17.337 ± 0.049	17.422 ± 0.103
52	NGC5845	19.470 ± 0.060	18.290 ± 0.030	14.860 ± 0.010	12.990 ± 0.010	12.150 ± 0.010	11.710 ± 0.010	11.430 ± 0.010
53	PGC1218738	18.268 ± 0.025		17.104 ± 0.034	15.912 ± 0.008	15.464 ± 0.014	15.441 ± 0.028	15.092 ± 0.039
54	PGC1191322		21.423 ± 0.142	19.157 ± 0.084	17.625 ± 0.009	16.944 ± 0.008	16.621 ± 0.010	16.417 ± 0.029
55	PGC1215798	17.434 ± 0.016	17.182 ± 0.011	17.101 ± 0.022	16.283 ± 0.005	16.055 ± 0.006	16.005 ± 0.008	15.854 ± 0.035
56	NGC5846+A	17.050 ± 0.050	16.060 ± 0.030	12.460 ± 0.010	10.570 ± 0.010	9.770 ± 0.010	9.300 ± 0.010	9.000 ± 0.010
57	NGC5846	17.120 ± 0.050	16.100 ± 0.030	12.800 ± 0.010	10.840 ± 0.010	9.980 ± 0.010	9.470 ± 0.010	9.240 ± 0.010
58	SDSSJ150634.25+001255.6		22.701 ± 0.345	18.881 ± 0.077	17.597 ± 0.010	17.030 ± 0.010	16.768 ± 0.012	16.701 ± 0.054
59	PGC3119319	22.363 ± 0.147	21.303 ± 0.089	17.892 ± 0.018	15.857 ± 0.003	15.011 ± 0.003	14.573 ± 0.003	14.220 ± 0.004
60	NGC5841	21.160 ± 0.140	19.070 ± 0.040	15.670 ± 0.010	14.030 ± 0.010	13.260 ± 0.010	12.820 ± 0.010	12.650 ± 0.010
61	PGC1156476		21.833 ± 0.377	19.121 ± 0.063	17.715 ± 0.009	17.069 ± 0.008	16.800 ± 0.010	16.607 ± 0.034
62	PGC1171244	20.682 ± 0.081	20.226 ± 0.054	18.850 ± 0.061	17.661 ± 0.010	17.224 ± 0.010	16.997 ± 0.015	16.930 ± 0.055
63	NGC5846:[MTT2005]226	21.704 ± 0.145	21.268 ± 0.104	19.455 ± 0.128	18.329 ± 0.017	17.842 ± 0.026	17.589 ± 0.022	17.354 ± 0.077
64	NGC5850	15.110 ± 0.050	14.730 ± 0.030	13.038 ± 0.010	11.530 ± 0.010	10.960 ± 0.010	10.560 ± 0.010	10.520 ± 0.010
65	PGC1185172		22.125 ± 0.567	18.628 ± 0.075	17.330 ± 0.009	16.784 ± 0.009	16.526 ± 0.011	16.310 ± 0.028
66	PGC054004	23.673 ± 0.372		17.305 ± 0.037	15.685 ± 0.004	14.985 ± 0.004	14.621 ± 0.004	14.460 ± 0.013
67	NGC5854	19.480 ± 0.060	17.140 ± 0.030	13.950 ± 0.010	12.340 ± 0.010	11.640 ± 0.010	11.230 ± 0.010	11.070 ± 0.010
68	PGC054016			16.938 ± 0.025	15.607 ± 0.003	14.954 ± 0.003	14.613 ± 0.003	14.441 ± 0.009
69	PGC1217593		21.631 ± 0.128	18.972 ± 0.069	17.578 ± 0.009	16.915 ± 0.008	16.578 ± 0.009	16.439 ± 0.045
70	PGC054037			17.274 ± 0.028	15.586 ± 0.004	14.796 ± 0.004	14.419 ± 0.005	14.159 ± 0.013
71	NGC5846:[MTT2005]258	22.202 ± 0.150		20.798 ± 0.565	18.820 ± 0.032	18.363 ± 0.033	18.273 ± 0.046	19.024 ± 0.365
72	NGC5846:[MTT2005]259			20.699 ± 0.413	19.421 ± 0.028	18.579 ± 0.036	18.594 ± 0.059	19.142 ± 0.368
73	PGC054045			18.066 ± 0.073	16.316 ± 0.007	15.630 ± 0.007	15.329 ± 0.018	15.121 ± 0.021
74	SDSSJ150812.35+012959.7			19.487 ± 0.180	17.743 ± 0.014	17.059 ± 0.012	16.705 ±	

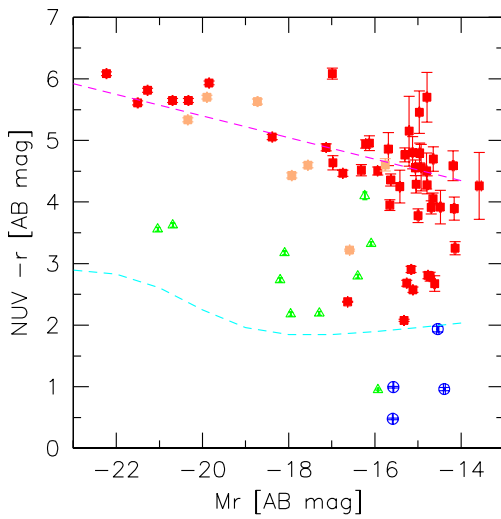
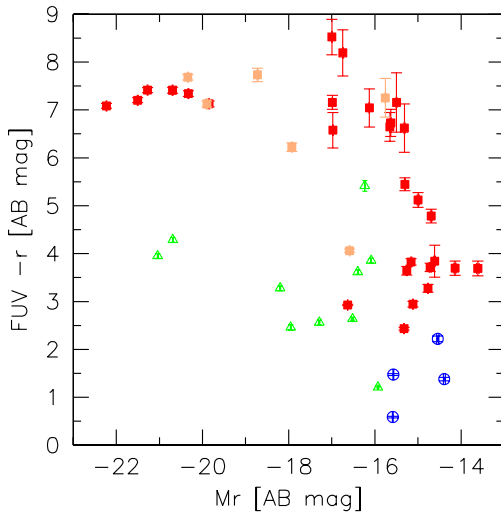


**Figure 6.** UV – optical CMDs of NGC 5846. Top:  $M_r$  versus  $FUV-r$ . Bottom:  $M_r$  versus  $NUV-r$ . In the  $M_r$  versus  $NUV-r$  CMD, we over-plot the Wyder et al. (2007) fits to the red and blue galaxy sequences. Green triangles mark Spirals, Ellipticals and S0s are indicated with red and orange squares, respectively, and blue circles show Irregulars. The magnitudes were corrected by Galactic extinction (Burstein & Heiles 1982).

by both Ellipticals and S0s. ETGs represent 82 per cent (56/69) of the total galaxy population and 79 per cent (44/56) of them are dwarfs. The 33 per cent (14/44) of galaxies fainter than  $Mr = -18$  are ETGs lying in the “green valley”, i.e. with  $2 \leq NUV-r \leq 4$ , some of them very near to the blue sequence. This behaviour agrees with the findings of Mazzei et al. (2014). These authors, studying the evolution of ETGs in two groups of the Leo cloud, USCG U376 and LGG 225, found that rejuvenation

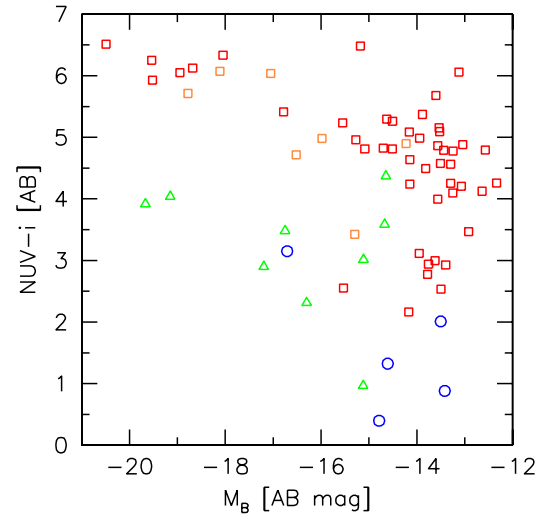


**Figure 7.** Top: The  $M_B$  versus  $NUV-i$  CMD of the group members. Symbols are as in Fig. 6. Bottom: Cumulative distributions of  $NUV-i$  of dwarf ( blue dashed line) and normal ( red continuous line) ETGs in our group; according to the Kolmogorov-Smirnov test the null hypothesis, that the two distributions are drawn from a same parent distribution, can be rejected at a confidence level  $> 99$  per cent.

episodes are more frequent in fainter ETGs (see their Fig. 5).

Figure 7 shows the absolute B magnitude,  $M_B$ , versus  $NUV-i$  of the group members (top panel). In the bottom panel of Figure 7, the cumulative distribution of  $NUV-i$  for normal and dwarf members of the group is shown. The distribution gives the fraction of normal and dwarf galaxies in the group that have a colour greater (redder) than a given value of  $NUV-i$ . For example,  $\sim 90$  and 20 per cent of normal and

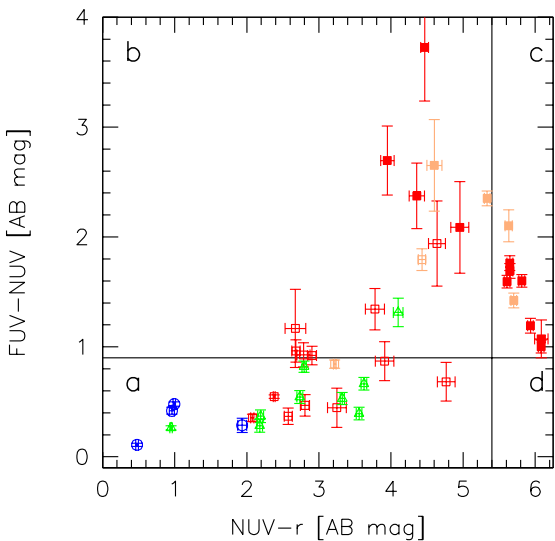


**Figure 8.** The FUV–NUV versus NUV–r colour–colour diagram of the NGC 5846 group members. Symbols are as in the previous figures. The magnitudes were corrected by Galactic extinction following Burstein & Heiles (1982). Solid lines correspond to  $\text{FUV}-\text{NUV} < 0.9$ , i.e. UV rising slope, and  $\text{NUV}-\text{r} > 5.4$ , i.e. a galaxy devoid of young massive stars. These conditions, following the UV classification scheme by Yi et al. (2011), separate passive evolving ETGs (region b) from star forming galaxies (region a), see text). Filled symbols are for galaxies with  $\text{FUV}-\text{r} \geq 6.6$  mag

dwarf galaxies, respectively, have  $\text{NUV}-\text{i} > 5$ . According to the Kolmogorov-Smirnov test, the null hypothesis that two distributions are drawn from the same parent distribution can be rejected at a confidence level  $> 99$  per cent. We consider the hypothesis that giant ETGs members may either have formed through or have experienced a significant number of accretions of dwarfs galaxies during the evolution of the group. In this hypothesis the color distributions of the two samples should have similar characteristics.

This should be particularly true if the accretions have been “dry”, i.e. the accretion has been “sterile” not igniting star formation episodes.

The statistically significant difference of the  $\text{NUV-i}$  of dwarfs and giant ETGs rules out the above formation scenario and a “dry” accretion scenario. Instead, we suggest that in the star formation history of both dwarfs and normal ETGs, gas dissipation cannot be neglected. We further explore this hypothesis in the following section.

#### 4.3 The colour–colour FUV–NUV versus NUV–r diagram

The slope of the UV spectrum is related to the temperature of the stars emitting in the UV and their relative contribution to the total flux. The value  $\text{FUV}-\text{NUV} = 0.9$  indicates a flat UV spectrum in the  $\lambda$ – versus  $F_\lambda$  domain, whereas a negative  $\text{FUV}-\text{NUV}$  corresponds to a bluer population. Yi et al. (2011) established a colour criterion to classify ETGs according to their UV spectral morphology based on three colour. Passively evolving ETGs would have

$\text{NUV}-\text{r} \geq 5.4$ , and  $\text{FUV}-\text{r} \geq 6.6$ . These values indicate the average value of the red sequence in Fig. 6. ETGs showing UV upturn with no residual star formation have to obey a further condition,  $\text{FUV}-\text{NUV} < 0.9$ . Figure 8 shows the position of NGC 5846 group members in the colour–colour UV–optical diagram emphasising their morphological classification. The same fraction of dwarf ETGs which stays in the “green valley” of Fig. 6, i.e. 33 per cent, lies in the region where residual star formation is expected (region a in Fig. 8), in good agreement with findings of Mazzei et al. (2014). All the ETGs brighter than  $-18$  in the r-band (Fig. 6, top panel) show red  $\text{FUV}-\text{r}$  colours and  $\text{FUV}-\text{NUV} > 0.9$  and lie in the regions b) and c) of Fig. 8. The brightest members of this group, i.e., NGC 5846 and NGC 5813, lie in the right upper region of this colour–colour diagram, i.e. region c), where passively evolving ETGs would stay according the Yi et al. (2011) criterion. No galaxies are found in region d) of Fig. 8, where ETGs with UV upturn and no residual star formation would lie.

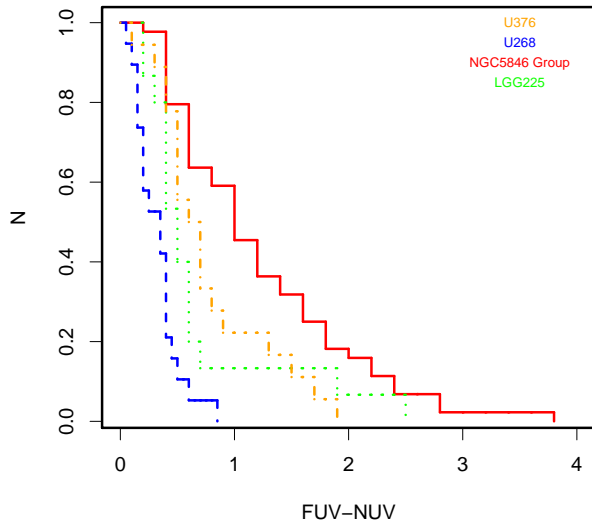
## 5 COMPARISON WITH OTHER GROUPS AND THE VIRGO CLUSTER

Figure 9 shows the cumulative distribution of the  $\text{FUV}-\text{NUV}$  colours of NGC5846, and of three groups already analysed in the Leo cloud (Paper I and II). This figure points out that the fraction of red UV colours, i.e.  $\text{FUV}-\text{NUV} > 0.9$ , increases with increasing number of ETGs. By comparing Fig. 6 (bottom) with Figures 10 and 11 in Marino et al. (2013) we note that the number of galaxies with red  $\text{NUV}-\text{r}$  colours, i.e. along the red sequence, all ETGs, increases with the groups are more massive and composed by more galaxies.

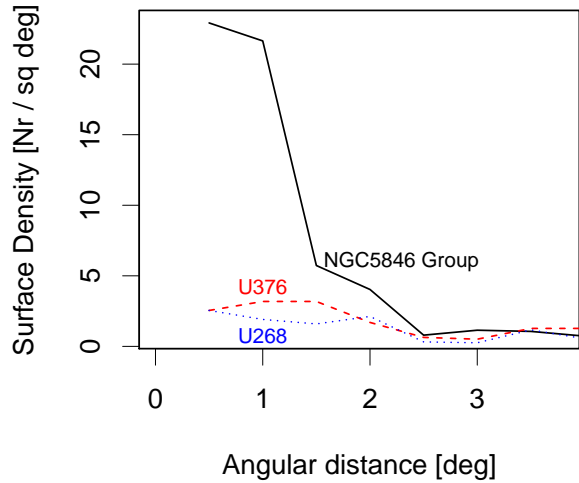
Figure 10 compares the density distribution versus angular distance from the dynamical centre of NGC 5486 (solid line) with the density distribution of the groups previously studied, i.e., USGC U376 (dashed line) and USGC U268 (dotted line). These latter groups are located in the Leo cloud. The dynamical analysis by Marino et al. (2014) suggests that USGC U268 is in a pre-virial collapse phase while U376 seems in a more evolved phase toward virialization. Notice that our distribution is different from that shown in Mahdavi et al. (2005, their Figure 7) because we use the centre of mass of the group (Table 2) as centre of the density distribution. We obtain the same distribution as Mahdavi et al. (2005) if we select NGC 5486 as centre of the group.

Figure 11 shows the UV luminosity function (LF hereafter; top panel FUV and bottom panel NUV) of NGC 5846 group. For comparison we plot, on the same scale, the UV LFs of the Virgo cluster (dotted line) as in Figure 8 of Boselli & Gavazzi (2014). These authors noted that the NUV and FUV LFs of Virgo and the field are similar. We find that FUV and NUV LFs of NGC 5846 group are quite similar to those of the Virgo cluster. In particular, as shown in Fig. 12, also the LFs of late type galaxies and ETGs in both groups are quite indistinguishable from those of this cluster.

Figure 13 shows that the shape of the FUV and NUV LFs in less dense groups (see Figure 10) is dominated by late-type galaxies. In the brightest magnitude bins, late type



**Figure 9.** Cumulative distribution of FUV–NUV colours of galaxies in NGC5846 group (solid line), and in three groups previously studied, i.e. U268 (dashed line), U376 (dot-dashed line), and LGG225 (dotted line).



**Figure 10.** Surface member density as a function of the radial distance from the centre of mass defined by the dynamical analysis developed in Section 2.4. For comparison the surface density distributions of the two groups U268 (dotted line) and U376 (dashed line) are shown.

galaxies are more numerous in these groups than in denser groups like NGC 5846 and Virgo.

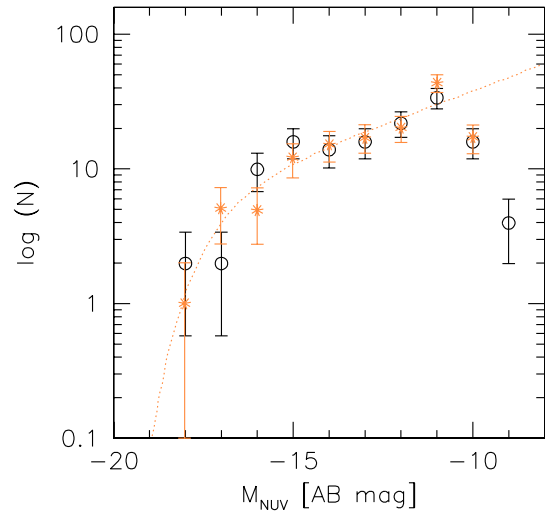
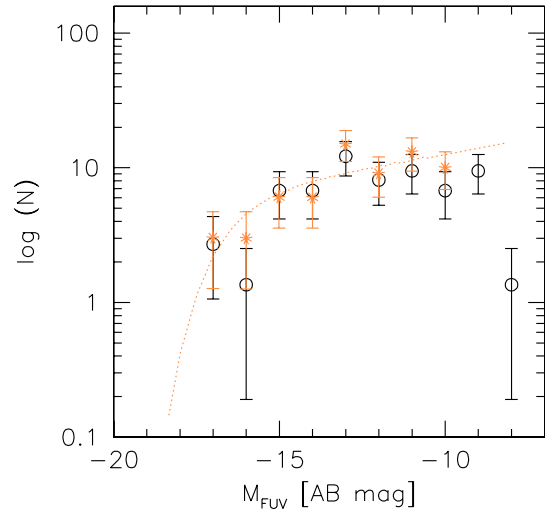


**Figure 11.** The FUV and NUV LFs of NGC 5846 group (open circles) compared to those of the Virgo cluster (asterisks; dotted line shows the fit limited to -13 mag by Boselli & Gavazzi (2014)). LFs have been normalized to include the same galaxy number as Virgo, i.e., 135 in NUV and 65 in FUV as in Boselli & Gavazzi (2014).

## 6 SUMMARY AND CONCLUSIONS

This paper is the third of a series dedicated to the study of nearby groups with a different morphological mix of galaxy populations and sampling different dynamical phases.

We have obtained FUV and NUV *GALEX* and SDSS -  $u, g, r, i, z$  AB magnitudes of 90 spectroscopically confirmed members of NGC 5846, the third most massive nearby association after Virgo and Fornax nearby clusters. The backbone of the group comes from the catalog of Ramella et al.

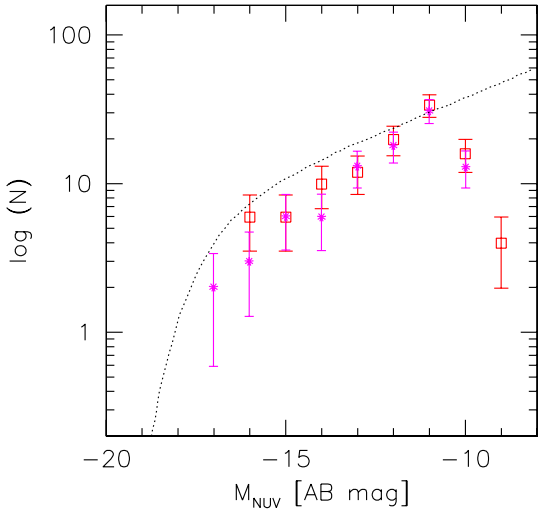
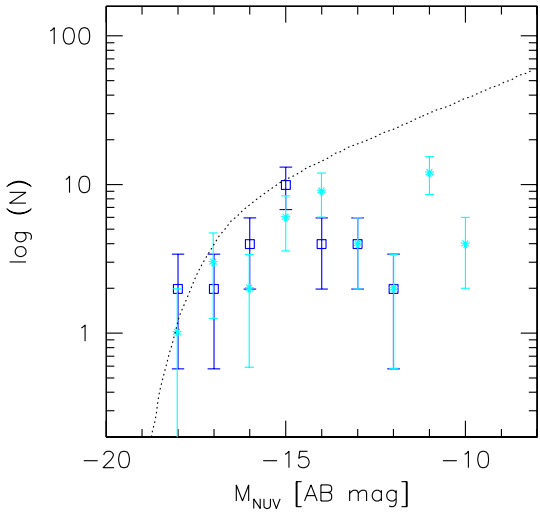


**Figure 12.** The NUV LFs of NGC 5846 group splitted in late type galaxies (top), and ETGs (bottom), compared to those of the Virgo cluster (asterisks and dotted line as in Fig.11) from Boselli & Gavazzi (2014, their Fig. 14).

(2002) that we enriched of members applying kinematical and dynamical selection criteria to galaxies with known optical redshift (see also Paper I and II).

The group membership as well as the characteristics of the group have been already investigated with a different method by Mahdavi et al. (2005) and Eigenthaler & Zeilinger (2010). Our selection of 90 members includes all the spectroscopically confirmed members of Mahdavi et al. (2005) and Eigenthaler & Zeilinger (2010) plus two ETGs in HYPERLEDA meeting our criteria.

The kinematical and dynamical analysis of the group indicates that it is in a evolved phase according to

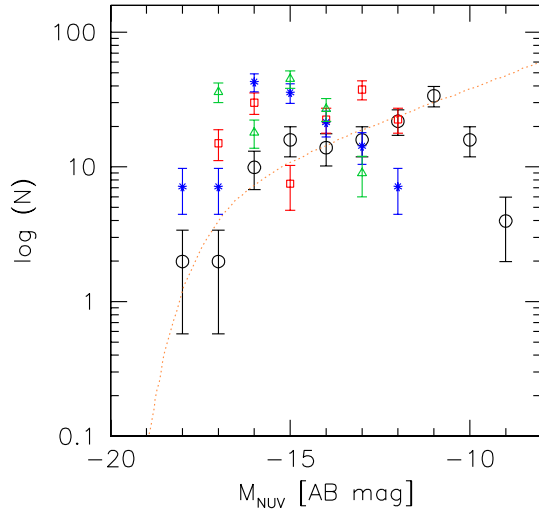
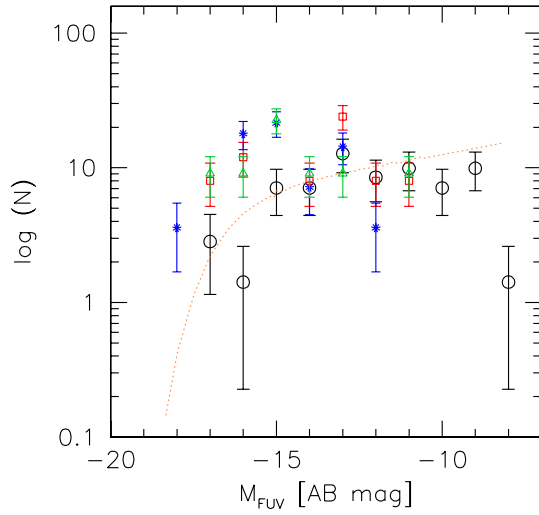


**Figure 13.** The FUV and NUV LFs of NGC 5846 group (circles) compared to those of the Virgo cluster (dotted line Boselli & Gavazzi (2014)), U376 (red squares), U268 (blue asterisks) and LGG225 (green triangles). LFs have been normalized as in Fig. 11.

Mahdavi et al. (2005) analysis. The main novelty of the present study is the UV analysis. Our analysis of the UV data shows that a large fraction of dEs (33 per cent, Section 4.3) does not reside in the red or in the blue sequence of the group CMD but it lies in the “green valley”, where “rejuvenation” episodes of dEs occur with higher frequency (Mazzei et al. 2014). We find that only 5 per cent of the total ETG population of the group lies in the region of passively evolving ETGs (Section 4.3, region c, Fig. 8) whereas dEs are found in the locus of star forming galaxies (region a, Fig. 8). Moreover, by analysing the cumulative NUV-i colour distributions of dEs and normal ETGs in the group,

the hypothesis that the two distributions are drawn from the same parent distribution can be rejected at a confidence level of  $>99$  per cent. We concluded that the UV-optical colours of normal ETGs in the group cannot be accounted by dry mergers of the dE population: gas dissipation, i.e. star formation, cannot be neglected in the evolution of the group members.

Boselli & Gavazzi (2014) found that Virgo galaxies are quenched by ram pressure and suggest that the quenching of the star formation activity in dwarf systems and the formation of the faint end of the red sequence is a very recent phenomenon. Although the UV LFs of both Virgo and NGC 5846 are very similar, only a small fraction of galaxies in NGC 5846 is passively evolving. Our UV-optical analysis suggests that star formation events are still occurring in this group, in particular in its dwarf ETG population, tracing a picture of a still active phase notwithstanding its large number of ETGs and its likely virialized configuration (Table 2).

Mazzei et al. (2014), investigating the evolution of the brightest ETGs in the U376 and LGG 225 groups, found that residual star formation, i.e. ‘rejuvenation’, is luminosity dependent so that bursts of star formation can occur still today in dEs, as found in this group.

In a forthcoming paper (Mazzei et al. 2016, in prep.), we will investigate further the evolution of the brightest ETG members and some dwarfs of this group using a smooth particle Hydrodynamic code with chemo-photometric implementation. We will also expand the study to other selected groups for which we have UV and optical images.

## ACKNOWLEDGMENTS

We acknowledge the usage of the HYPERLEDA and NED databases. Paola Mazzei and Roberto Rampazzo acknowledge support from INAF through grant PRIN-2014-14 ‘Star formation and evolution in galactic nuclei’.

Facilities: GALEX, Sloan

## REFERENCES

Adelman-McCarthy J. K., Agüeros M. A., Allam S. S., Alende Prieto C., Anderson K. S. J., Anderson S. F., Annis J., Bahcall N. A., 2008, *ApJS*, 175, 297

Balogh M. L., Baldry I. K., Nichol R., Miller C., Bower R., Glazebrook K., 2004, *ApJ*, 615, L101

Barnes J. E., 2002, *MNRAS*, 333, 481

Bianchi L., 2009, *Ap&SS*, 320, 11

Bianchi L., 2014, *Ap&SS*, 354, 103

Bianchi L., Efremova B., Herald J., Girardi L., Zabot A., Marigo P., Martin C., 2011, *MNRAS*, 411, 2770

Boselli A., Gavazzi G., 2014, *A&A Rev.*, 22, 74

Burstein D., Heiles C., 1982, *AJ*, 87, 1165

Cardelli J. A., Clayton G. C., Mathis J. S., 1989, *ApJ*, 345, 245

Davis M., Geller M. J., 1976, *ApJ*, 208, 13

Di Matteo T., Springel V., Hernquist L., 2005, in A. Meroni, S. Nayakshin, & R. A. Sunyaev ed., *Growing Black Holes: Accretion in a Cosmological Context* Black Holes in Galaxy Mergers, pp 340–345

Dressler A., 1980, *ApJ*, 236, 351

Dressler A., Shectman S. A., 1988, *AJ*, 95, 985

Efron B., 1982, *The Jackknife, the Bootstrap and other resampling plans*

Eigenthaler P., Zeilinger W. W., 2010, *A&A*, 511, A12

Eke V. R., Baugh C. M., Cole S., Frenk C. S., Norberg P., Peacock J. A., 2004, *MNRAS*, 348, 866

Ferguson H. C., Sandage A., 1990, *AJ*, 100, 1

Ferguson H. C., Sandage A., 1991, *AJ*, 101, 765

Firth P., Evstigneeva E. A., Jones J. B., Drinkwater M. J., Phillipps S., Gregg M. D., 2006, *MNRAS*, 372, 1856

Giuricin G., Marinoni C., Ceriani L., Pisani A., 2000, *ApJ*, 543, 178

Gómez P. L., Nichol R. C., Miller C. J., Balogh M. L., Goto T., Zabludoff A. I., Romer A. K., Bernardi M., Sheth R., Hopkins A. M., Castander F. J., Connolly A. J., Schneider D. P., Brinkmann J., Lamb D. Q., SubbaRao M., York D. G., 2003, *ApJ*, 584, 210

Goto T., Yamauchi C., Fujita Y., Okamura S., Sekiguchi M., Smail I., Bernardi M., Gomez P. L., 2003, *MNRAS*, 346, 601

Haynes M. P., Giovanelli R., 1991, *AJ*, 102, 841

Hou A., Parker L. C., Wilman D. J., McGee S. L., Harris W. E., Connelly J. L., Balogh M. L., Mulchaey J. S., Bower R. G., 2012, *MNRAS*, 421, 3594

Jedrzejewski R. I., 1987, *MNRAS*, 226, 747

Kawata D., Mulchaey J. S., 2008, *ApJ*, 672, L103

Lewis I., Balogh M., De Propris R., Couch W., et al. 2002, *MNRAS*, 334, 673

Machacek M. E., Jerius D., Kraft R., Forman W. R., Jones C., Randall S., Giacintucci S., Sun M., 2011, *ApJ*, 743, 15

Mahdavi A., Trentham N., Tully R. B., 2005, *AJ*, 130, 1502

Makarov D., Prugniel P., Terekhova N., Courtois H., Vauglin I., 2014, *A&A*, 570, A13

Mamon G. A., 1992, *ApJ*, 401, L3

Marino A., Bianchi L., Mazzei P., Rampazzo R., Galletta G., 2014, *Advances in Space Research*, 53, 920

Marino A., Bianchi L., Rampazzo R., Buson L. M., Bettoni D., 2010, *A&A*, 511, A29

Marino A., Plana H., Rampazzo R., Bianchi L., Rosado M., Bettoni D., Galletta G., Mazzei P., Buson L., Ambrocio-Cruz P., Gabbasov R. F., 2013, *MNRAS*, 428, 476

Martin D. C., Fanson J., Schiminovich D., et al. 2005, *ApJ*, 619, L1

Mazzei P., Marino A., Rampazzo R., 2014, *ApJ*, 782, 53

Moore B., Katz N., Lake G., Dressler A., Oemler A., 1996, *Nature*, 379, 613

Morrissey P., Conrow T., Barlow T. A., Small T., Seibert M., Wyder T. K., Budavári 2007, *ApJS*, 173, 682

Mulchaey J. S., Davis D. S., Mushotzky R. F., Burstein D., 2003, *ApJS*, 145, 39

Nolthenius R., 1993, *ApJS*, 85, 1

Perea J., del Olmo A., Moles M., 1990, *Ap&SS*, 170, 347

Poggianti B. M., von der Linden A., De Lucia G., et al. 2006, *ApJ*, 642, 188

Ramella M., Geller M. J., Pisani A., da Costa L. N., 2002, *AJ*, 123, 2976

Rampazzo R., Panuzzo P., Vega O., Marino A., Bressan A., Clemens M. S., 2013, *MNRAS*, 432, 374

Randall S. W., Forman W. R., Giacintucci S., Nulsen

P. E. J., Sun M., Jones C., Churazov E., David L. P., Kraft R., Donahue M., Blanton E. L., Simionescu A., Werner N., 2011, *ApJ*, 726, 86

Schawinski K., Kaviraj S., Khochfar S., Yoon S.-J., Yi S. K., Deharveng J.-M., Boselli A., Barlow T., et al. 2007, *ApJS*, 173, 512

Silverman B. W., 1986, Density estimation for statistics and data analysis

Tago E., Einasto J., Saar E., Tempel E., Einasto M., Vennik J., Müller V., 2008, *A&A*, 479, 927

Tammann G. A., 1994, in Meylan G., Prugniel P., eds, European Southern Observatory Conference and Workshop Proceedings Vol. 49 of European Southern Observatory Conference and Workshop Proceedings, Dwarf Galaxies in the Past. p. 3

Toomre A., Toomre J., 1972, *ApJ*, 178, 623

Trinchieri G., Goudfrooij P., 2002, *A&A*, 386, 472

Tully R. B., 1987, *ApJ*, 321, 280

Tully R. B., 1988, *Nearby galaxies catalog*. Cambridge and New York, Cambridge University Press, 1988, 221 p.

Werner N., Oonk J. B. R., Sun M., Nulsen P. E. J., Allen S. W., Canning R. E. A., Simionescu A., Hoffer A., Connor T., Donahue M., Edge A. C., Fabian A. C., von der Linden A., Reynolds C. S., Ruszkowski M., 2014, *MNRAS*, 439, 2291

Werner N., Zhuravleva I., Churazov E., Simionescu A., Allen S. W., Forman W., Jones C., Kaastra J. S., 2009, *MNRAS*, 398, 23

Yi S. K., Lee J., Sheen Y.-K., Jeong H., Suh H., Oh K., 2011, *ApJS*, 195, 22

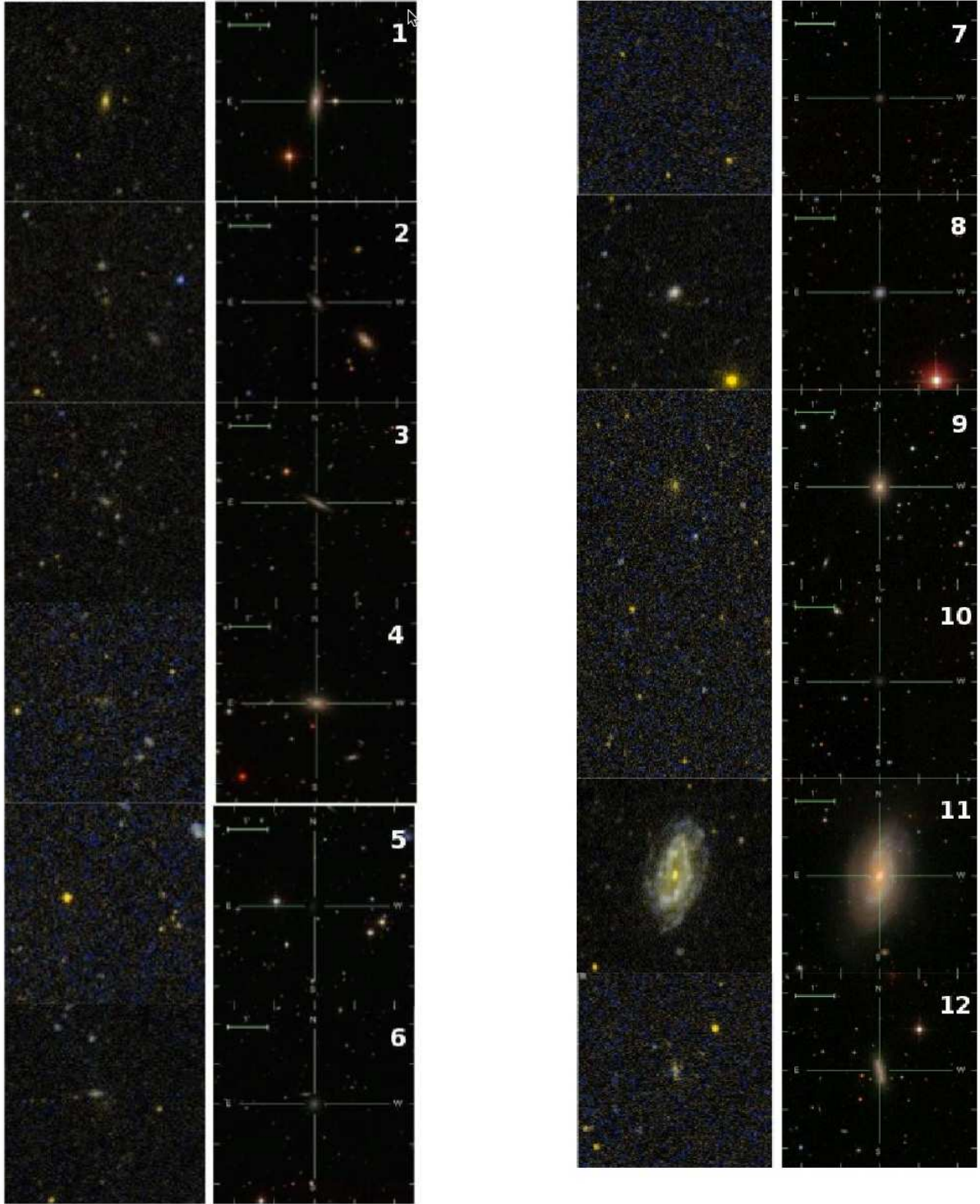
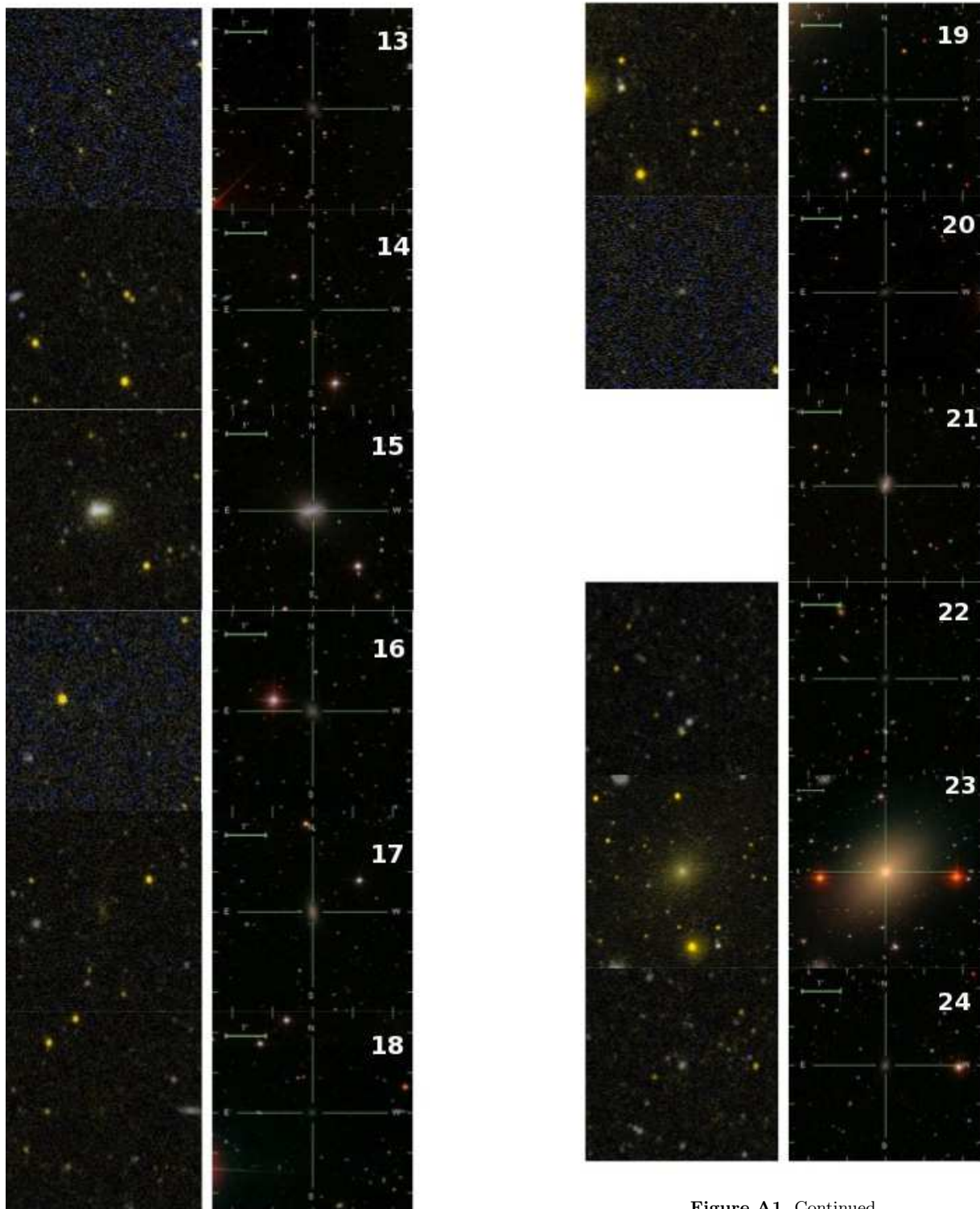


Figure A1. Continued.

**Figure A1.** UV (FUV, blue, NUV, yellow, left) and optical (SDSS: g, r, i are blue, green and red, respectively, right) images of members of NGC 5846.

#### APPENDIX A: UV AND OPTICAL IMAGES OF GALAXIES IN NGC 5846

Figures A1 show the UV and optical colour composite images of the members of NGC 5846. The size of each image is  $5 \times 5$  arcmin. One arcmin (bar shown) corresponds to  $\approx 7$  kpc at the distance of the group.



**Figure A1.** Continued.

**Figure A1.** Continued.

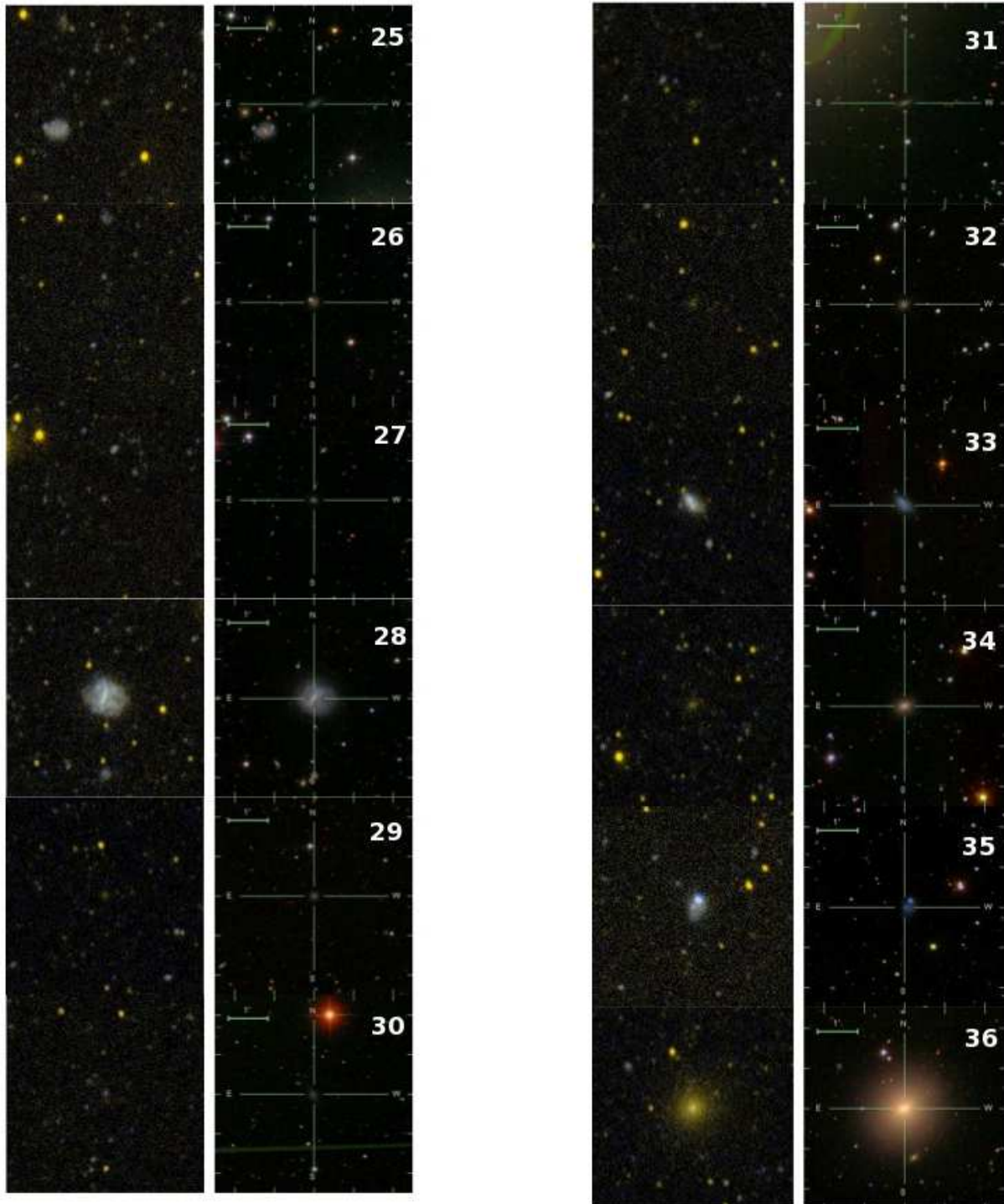


**Figure A1.** Continued.

**Figure A1.** Continued.

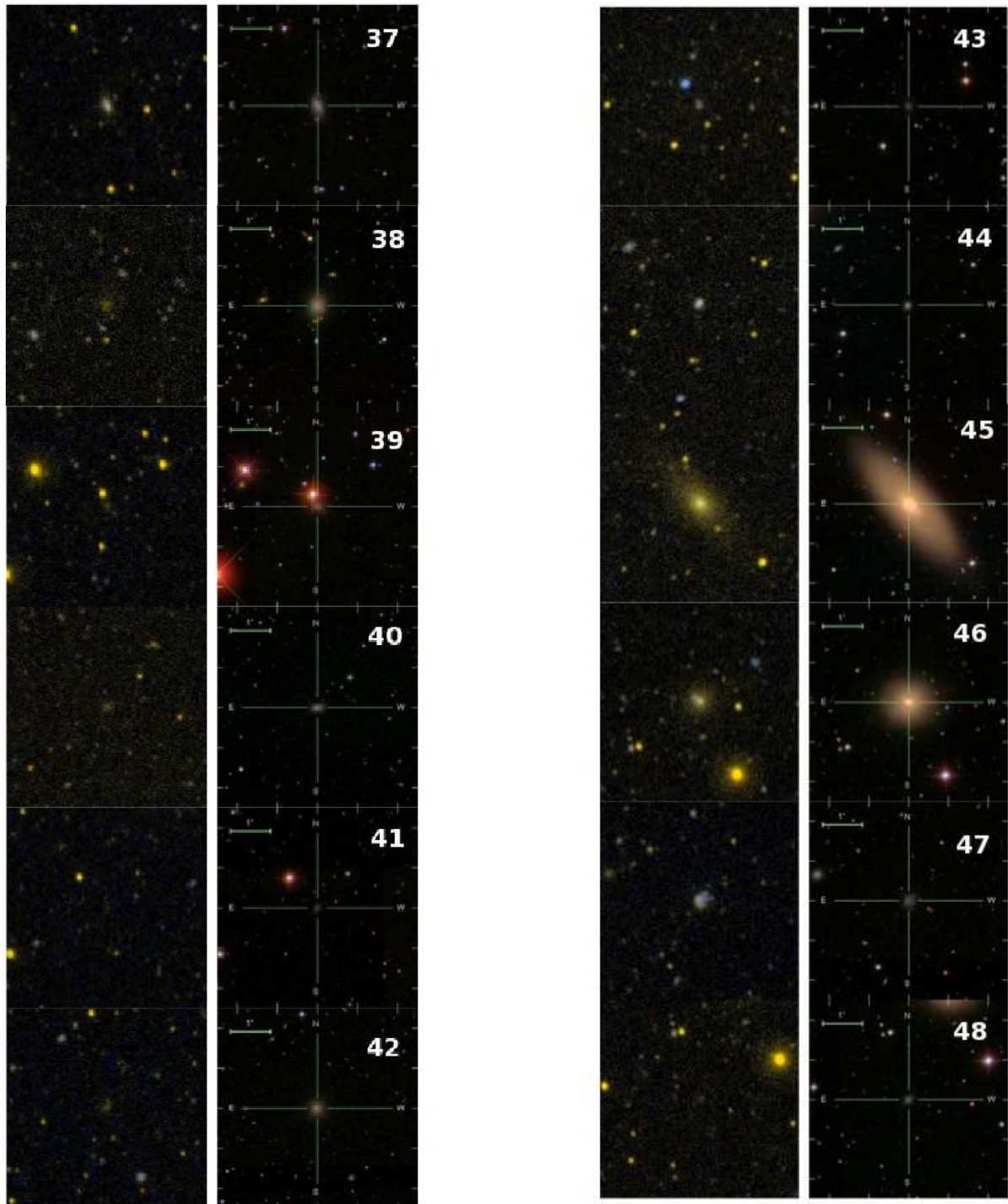


**Figure A1.** Continued.

**Figure A1.** Continued.

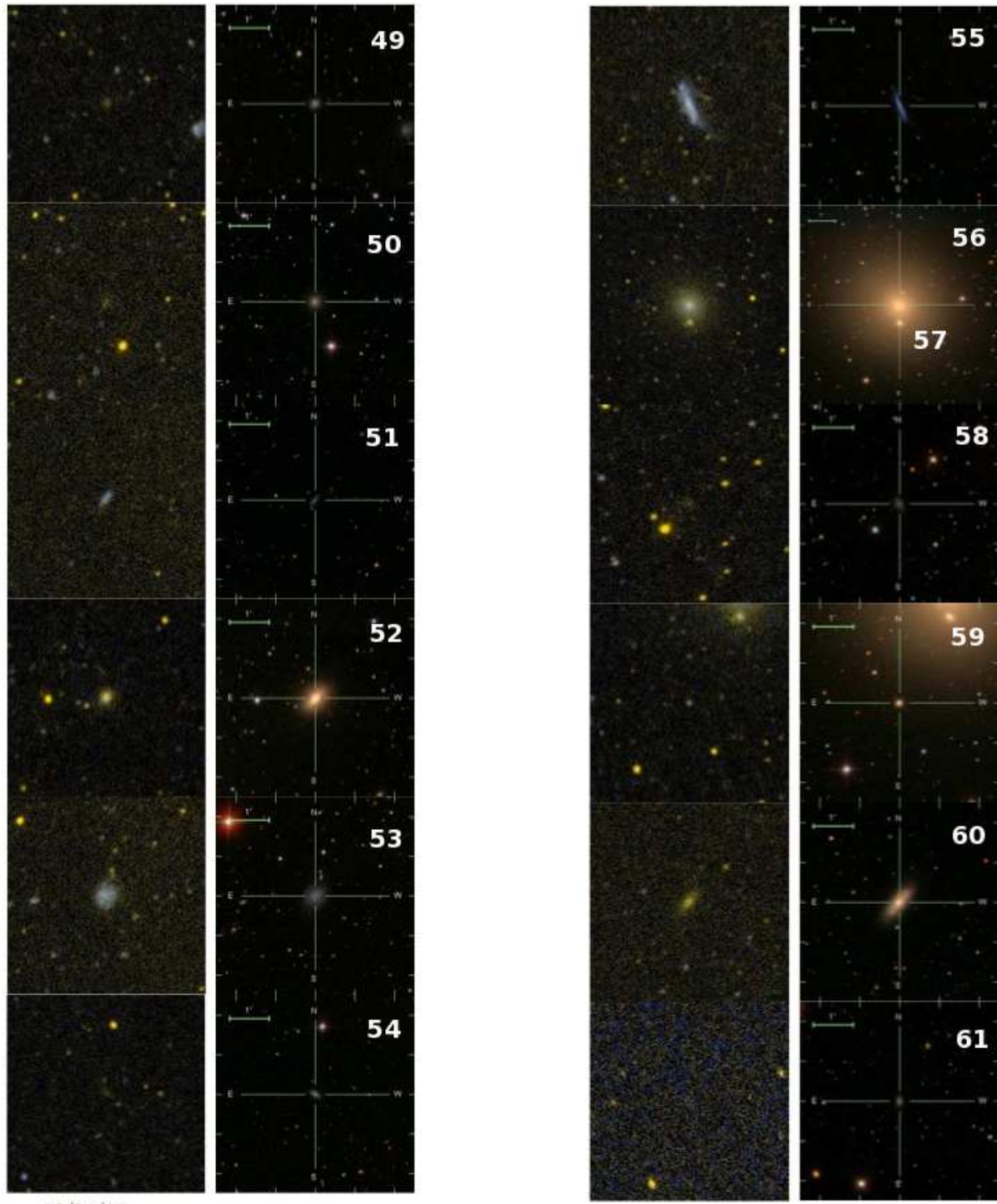
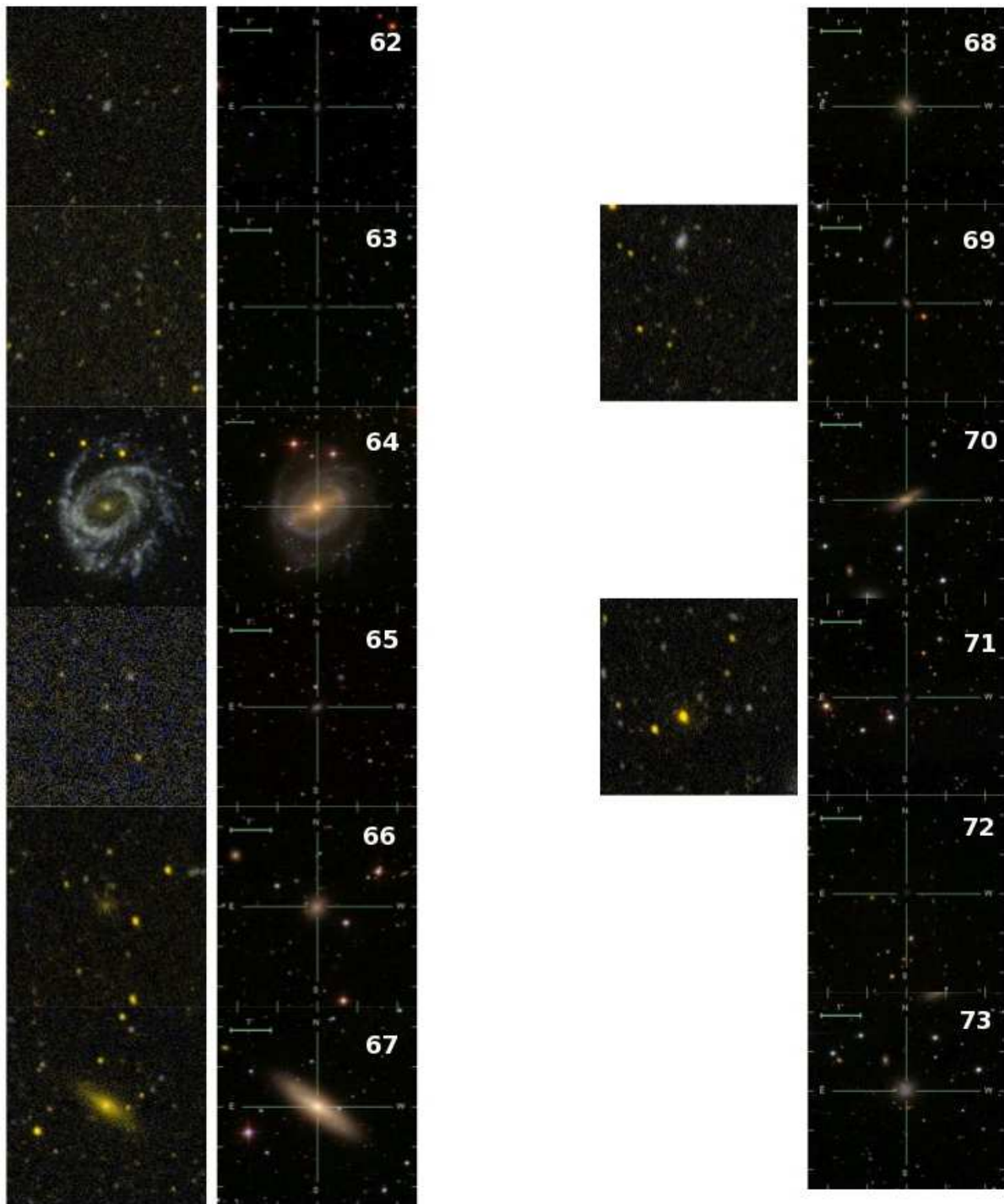


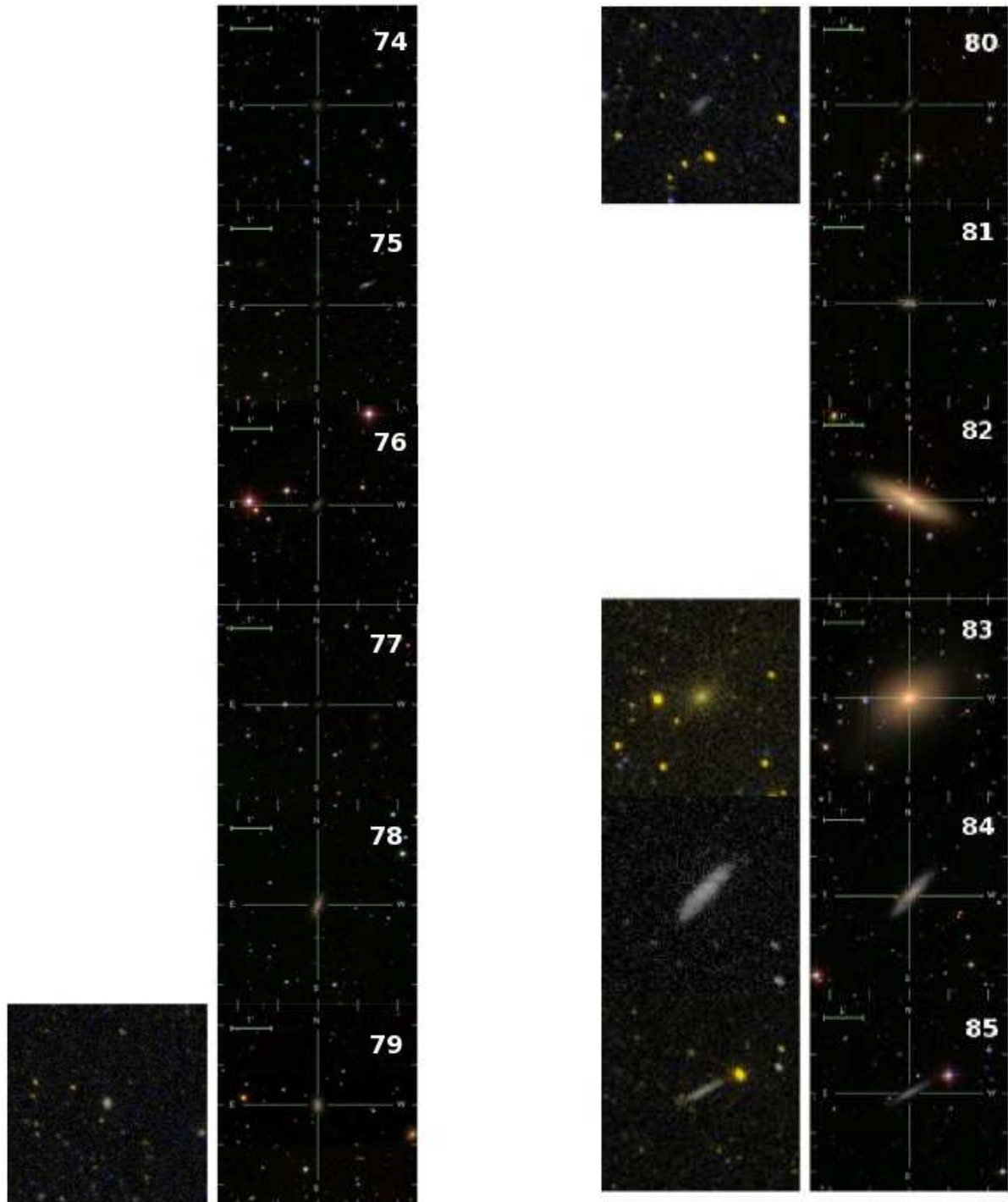
Figure A1. Continued.

Figure A1. Continued.



**Figure A1.** Continued.

**Figure A1.** Continued.



**Figure A1.** Continued.

**Figure A1.** Continued.

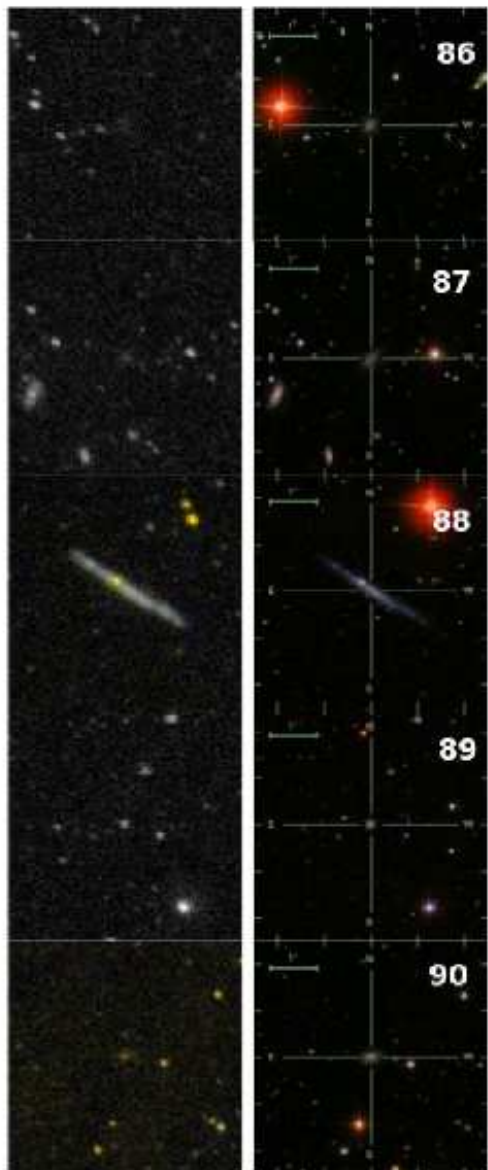


**Figure A1.** Continued.

**APPENDIX B: THE ENVIRONMENT OF NGC  
5846**

**Table B1.** Galaxies in a box of  $4 \text{ Mpc} \times 4 \text{ Mpc}$  centered on NGC 5846 with heliocentric velocity between 807 and 2600 km/s.

Galaxies	RA (J2000) (h)	Dec. (J2000) (deg)	Morph. type	Mean Vel. [km/s]	logD <sub>25</sub> [arcmin]	logr <sub>25</sub>	P.A. [deg]	B <sub>T</sub> mag
PGC1150067	14.80685	-0.17365		$2350 \pm 60$	0.34	0.07	68	$18.83 \pm 0.33$
SDSSJ144834.42+052552.5	14.80956	5.43127		$1698 \pm 1$			153.9	$18.18 \pm 0.5$
PGC1241857	14.8397	2.95819		$1697 \pm 1$	0.56	0.21	166.7	$17.18 \pm 0.67$
SDSSJ145059.85+022016.4	14.84996	2.3379		$1528 \pm 24$	0.49	0.12	107.3	$18.56 \pm 0.35$
SDSSJ145106.77+023127.0	14.85189	2.52415		$2071 \pm 3$	0.49	0.09	79.3	$18.53 \pm 0.29$
SDSSJ145201.94+025841.8	14.86721	2.97824		$1814 \pm 2$	0.45	0.02	17.86	$\pm 0.35$
NGC5768	14.86887	-2.52976	5.3	$1947 \pm 8$	1.11	0.12	110.9	$13.52 \pm 0.5$
SDSSJ145243.39+043616.7	14.8787	4.60467		$1589 \pm 8$	0.8	0.49	98.7	$17.96 \pm 0.5$
IC1066	14.88413	3.29601	3.2	$1567 \pm 4$	1.08	0.26	69.5	$14.27 \pm 0.28$
IC1067	14.88479	3.33175	3	$1566 \pm 4$	1.26	0.09	129	$13.62 \pm 0.29$
NGC5770	14.88751	3.95977	-2	$1477 \pm 15$	1.04	0.09		$13.18 \pm 0.24$
NGC5774	14.89514	3.58253	6.9	$1566 \pm 2$	1.23	0.21	116.7	$13.1 \pm 0.51$
IC1070	14.89759	3.48472	2.4	$1677 \pm 15$	0.89	0.4	121.7	$15.94 \pm 0.66$
NGC5775	14.89933	3.54426	5.2	$1676 \pm 2$	1.57	0.64	148.9	$12.23 \pm 0.13$
PGC1223887	14.90956	2.34392		$2158 \pm 42$	0.56	0.27	2.4	$18.36 \pm 0.47$
PGC135871	14.91193	1.16187	10	$1830 \pm 7$				$17.8 \pm 0.35$
PGC1197564	14.91551	1.52556		$1759 \pm 8$	0.49	0.11	70.6	$18.77 \pm 0.87$
PGC1184577	14.91925	1.10064		$1715 \pm 3$	0.4	0.18	9.9	$18.35 \pm 0.28$
PGC053365	14.92858	-1.00899	9	$1849 \pm 2$	0.8	0.21	43.2	$15.78 \pm 0.37$
UGC09601	14.93383	-1.38787	5.9	$1862 \pm 8$	1.09	0.11	171.7	$14.62 \pm 0.38$
PGC1083529	14.93898	-2.76159		$1888 \pm 9$	0.41	0.06	85.4	$18.66 \pm 0.3$
PGC184824	14.96245	-2.98707	1.6	$1800 \pm 64$	0.61	0.13	130.7	$17.14 \pm 0.37$
PGC184842	14.96883	-1.31237	3.8	$1947 \pm 7$	0.75	0.33	149.5	$16.45 \pm 0.31$
NGC5792	14.97296	-1.09093	3	$1924 \pm 2$	1.55	0.41	88.5	$12.12 \pm 0.12$
PGC053577	15.00036	-1.09107	10	$1886 \pm 2$	0.66	0.03		$15.81 \pm 0.36$
UGC09682	15.07505	-0.85135	8.6	$1810 \pm 4$	1.21	0.6	175.2	$15.43 \pm 0.36$
PGC2801020	15.07616	-2.587	10	$1624 \pm 2$	0.89	0.14	147.8	$16.51 \pm 0.32$
PGC1085904	15.11893	-2.66278		$2042 \pm 1$	0.53	0.18	93.2	$17.92 \pm 0.3$
PGC1128787	15.15933	-1.02163		$1858 \pm 1$	0.5	0.19	133	$17.56 \pm 0.35$
PGC054159	15.17978	-0.34824	6	$2159 \pm 2$	0.91	0.6	86	$16.25 \pm 0.57$
PGC1176138	15.20881	0.81256	10	$1844 \pm 5$	0.89	0.31	118.1	$16.32 \pm 0.29$
PGC1200646	15.2115	1.62325		$1873 \pm 4$	0.62	0.31	56.3	$17.25 \pm 0.3$
PGC258278	15.2125	6.16417		$1487 \pm 8$				$\pm$
PGC1236445	15.25262	2.75183		$1764 \pm 3$	0.78	0.3	56.8	$16.89 \pm 0.49$
PGC054452	15.25961	2.24823	-1	$1906 \pm 2$	0.98	0.1	107.5	$14.82 \pm 0.34$
UGC09787	15.2619	1.45576	9	$1589 \pm 5$	1	0.23	46.9	$15.4 \pm 0.36$
PGC1234821	15.26832	2.69196		$1463 \pm 2$	0.72	0.62	169	$17.23 \pm 0.45$
PGC3124577	15.29151	3.58548		$1883 \pm 3$	0.58	0.04		$17.36 \pm 0.35$
PGC1168006	15.31585	0.51564		$2083 \pm 14$	0.49	0.25	141	$18.16 \pm 0.33$
PGC1230249	15.32038	2.54503	4.2	$1877 \pm 4$	0.72	0.18	49.5	$16.17 \pm 0.35$
PGC091432	15.32997	3.97806	7.9	$1712 \pm 8$	0.7	0.63	56	$\pm$
NGC5913	15.34873	-2.57796	1	$2002 \pm 5$	1.27	0.39	173.5	$14.02 \pm 0.38$
NGC5921	15.36568	5.07041	4	$1430 \pm 23$	1.48	0.17	140	$11.68 \pm 0.1$
PGC258471	15.37742	5.82917		$1796 \pm 8$				$\pm$
UGC09830	15.38356	4.52917	5.9	$1830 \pm 5$	0.79	0.39	33	$15.91 \pm 0.62$
PGC3123131	15.41392	3.08141		$1754 \pm 1$	0.5	0.15	83.5	$17.58 \pm 0.35$